DEFENCE R&D DÉFENSE

A Comparison Between a First-Order Closure Model for Disturbed Urban Canopy Flows with Observations for Mean Wind and Turbulence

Eugene Yee
Defence Research Establishment Suffield

John D. Wilson
University of Alberta

Defence R&D Canada

Technical Report

DRES TR 2001-058

December 2001

National Defence Défense nationale

Canada

A Comparison Between a First-Order Closure Model for Disturbed Urban Canopy Flows with Observations for Mean Wind and Turbulence

Eugene Yee
Defence Research Establishment Suffield

John D. Wilson
University of Alberta

Defence Research Establishment Suffield

Technical Report

DRES TR 2001–058

December 2001

This page intentionally left blank

List of Figures

This page intentionally left blank

List of Tables

This page intentionally left blank

Introduction

It is anticipated that there will be an increasing likelihood that Canadian forces in the foreseeable future will have to fight in or protect urban areas, whether in battle, peace-making, peace-keeping, or counter-terrorist operations. The increased awareness and importance accorded by the public worldwide and their governments to maintain appropriate defences against chemical and biological (CB) agents released in an urban environment, the prediction of casualties and human performance degradation resulting from such releases, and the development of operational procedures and regulations to control, mitigate, and monitor the fate of CB agents in urban areas with high population densities will require the development of physically-sound and fully-validated models for the disturbed wind flow and dispersion within an arbitrary domain inside a city (or, other built-up area).

In principle, particle trajectory (Lagrangian) dispersion models can be used to calculate dispersion in an urban environment provided the spatial pattern of mean wind and turbulence statistics over the urban landscape is known. Consequently, an understanding of the complex flow patterns which result from the interaction of the wind with clusters of buildings is required in order to predict the dispersion of harmful materials released in an urban environment. To assist in this understanding, there have been attempts to apply canopy flow models developed originally for vegetation (e.g., forests, crops, etc.) to the urban landscape. This is a natural development since vegetative canopy flow models, capable of reproducing many features of the velocity statistics needed in Lagrangian stochastic (LS) models, have been developed over the past thirty years with varying complexity, limitations, and successes. These models range from simple algebraic mixing length models [1],[2] to one- and two-equation prognostic models for the determination of the eddy viscosity [3],[4]. Second-order local closure models [5]–[7], and still higher-order models [8] have been developed for plant canopy flows. Although limitations of first-order closure models for canopy flows are well-recognized [9], they nevertheless are still widely employed. This is because these models provide both the simplicity and flexibility for describing many of the relevant turbulent processes in canopy flows, while enabling the solution of the resulting model equations to be computationally tractable (viz., second- and higher-order models are much more computationally demanding than first-order closure).

The primary objective of this study is to describe and investigate whether a simple first-order closure model for the prediction of the flow within and above a canopy (either vegetative or urban) yields mean velocity and second-order velocity statistics that are in close enough agreement with measurements so as to provide adequate input information for use

in Lagrangian dispersion models. For this purpose, a number of canopy experiments (some vegetative, but mostly urban) have been identified for use in model validation. We restrict our attention to experiments providing measurements of both the mean flow and the turbulence (turbulence kinetic energy, shear stress, and normal stresses), and depend heavily on high-quality data from wind tunnel and water channel studies.

Windflow model

A detailed explanation of the model equations and numerical procedure is given in Yee and Wilson [10], and so we shall give only a brief description here. In the so-called micro-scale (horizontal scales less than 2 km) resolution of atmospheric flow through an urban canopy, we solve the continuity equation (mass conservation) and the Reynolds-averaged Navier Stokes equations (momentum conservation) for steady and incompressible fluid flow under adiabatic conditions (neutrally-stratified atmosphere):

Continuity equation:

$$\frac{\partial U}{\partial x} + \frac{\partial V}{\partial y} + \frac{\partial W}{\partial z} = 0, \tag{1}$$

Reynolds-averaged Navier-Stokes equations:

$$\frac{\partial}{\partial x}(U^2 + \overline{u'^2}) + \frac{\partial}{\partial y}(UV + \overline{u'v'}) + \frac{\partial}{\partial z}(UW + \overline{u'w'}) = f(V - V_G) - \frac{\partial P}{\partial x} - C_d A U \sqrt{U^2 + V^2 + W^2}, \tag{2}$$

$$\frac{\partial}{\partial x}(UV + \overline{u'v'}) + \frac{\partial}{\partial y}(V^2 + \overline{v'^2}) + \frac{\partial}{\partial z}(VW + \overline{v'w'}) = f(U_G - U) - \frac{\partial P}{\partial y} - C_d A V \sqrt{U^2 + V^2 + W^2}, \tag{3}$$

and

$$\frac{\partial}{\partial x}(UW + \overline{u'w'}) + \frac{\partial}{\partial y}(VW + \overline{v'w'}) + \frac{\partial}{\partial z}(W^2 + \overline{w'^2}) = -\frac{\partial P}{\partial z} - C_d A W \sqrt{U^2 + V^2 + W^2}, \tag{4}$$

corresponding to the streamwise, cross-stream, and vertical mean momentum balance, respectively. Here, $\mathbf{x} \equiv (x_1, x_2, x_3) \equiv (x, y, z)$ is the position vector with the x-coordinate in the mean streamwise direction, the y-coordinate in the horizontal cross-stream direction, and the z-coordinate normal to the ground; $\mathbf{U} \equiv (U_1, U_2, U_3) \equiv (U, V, W)$ is the mean velocity vector with components in the x-, y-, and z-coordinates, respectively; $\mathbf{u}' \equiv (u'_1, u'_2, u'_3) \equiv (u', v', w')$ is the velocity fluctuation vector (departures from the mean velocity vector) in the x-, y-, and z-directions, respectively; P is the mean kinematic pressure; f is the Coriolis parameter defined as $f = 2\omega \sin\phi$, where ω is the magnitude of the angular velocity of the Earth's rotation, and ϕ is the latitude; C_d is the bulk drag coefficient assigned to either a single canopy element (obstacle) or a whole group of canopy elements; $A = A(x, y, z)$ is the frontal area per unit volume ($\mathrm{m}^2\ \mathrm{m}^{-3}$) of space occupied by either a single canopy element

or a whole group of canopy elements; and, an overbar is used to represent a Reynolds average. In Equations (2) and (3), the large-scale background horizontal kinematic pressure gradient P_b in the Planetary Boundary Layer (PBL) has been parameterized in terms of a nominal geostrophic wind aloft, so $fU_G = -\frac{\partial P_b}{\partial y}$ and $fV_G = \frac{\partial P_b}{\partial x}$, where (U_G, V_G) are the components of the geostrophic wind aloft.

The Reynolds-averaged Navier-Stokes equations (2) to (4) are not closed unless a model is provided which ties the kinematic (specific) Reynolds stress tensor $\overline{u_i' u_j'}$ $(i, j = 1, 2, 3)$ to the global history of the mean fluid velocity U_i in a physically consistent fashion. Herein lies the fundamental problem of turbulence. In order to compute all the mean-flow properties of the turbulent flow under consideration, we need a prescription for computing $\overline{u_i' u_j'}$. The specific Reynolds stresses appear in Equations (2) to (4) as spatial gradients and, physically, can be interpreted as forces "felt by" the mean flow. The simplest method for relating the Reynolds stresses to the mean velocity is to use the Boussinesq linear and isotropic eddy viscosity approximation

$$-\overline{u_i' u_j'} = 2KS_{ij} - \frac{2}{3}k\delta_{ij}, \tag{5}$$

where K is the eddy viscosity, k is the turbulence kinetic energy (TKE), $S_{ij} \equiv \frac{1}{2}\left(\frac{\partial U_i}{\partial x_j} + \frac{\partial U_j}{\partial x_i}\right)$ is the mean strain-rate tensor, and δ_{ij} is the Kronecker delta function. As a further simplification, we note that in most disturbed thin shear-layer flows (i.e., flows wherein shear strains $\ll$ normal strains), the normal stress gradients play a much smaller role than the shear stress gradients. In view of this, we will solve simplified U, V, W-momentum equations, that represent only what are (according to experience) the dominant terms (advection by the mean flow, pressure gradient, drag on obstacles, and the divergence of the shear stresses [turbulent momentum fluxes] in the three coordinate directions). With these simplifications, the mean momentum equations can be written explicitly as

$$\frac{\partial}{\partial x}\left(U^2 - K_a\frac{\partial U}{\partial x}\right) + \frac{\partial}{\partial y}\left(UV - K\left(\frac{\partial U}{\partial y} + \frac{\partial V}{\partial x}\right)\right) + \frac{\partial}{\partial z}\left(UW - K\left(\frac{\partial U}{\partial z} + \frac{\partial W}{\partial x}\right)\right) = f(V - V_G) - \frac{\partial P}{\partial x} - C_d A U\sqrt{U^2 + V^2 + W^2}, \tag{6}$$

$$\frac{\partial}{\partial x}\left(UV - K\left(\frac{\partial U}{\partial y} + \frac{\partial V}{\partial x}\right)\right) + \frac{\partial}{\partial y}\left(V^2 - K_a\frac{\partial V}{\partial y}\right) + \frac{\partial}{\partial z}\left(VW - K\left(\frac{\partial V}{\partial z} + \frac{\partial W}{\partial y}\right)\right) = f(U_G - U) - \frac{\partial P}{\partial y} - C_d A V\sqrt{U^2 + V^2 + W^2}, \tag{7}$$

and

$$\frac{\partial}{\partial x}\left(UW - K\left(\frac{\partial U}{\partial z} + \frac{\partial W}{\partial x}\right)\right) + \frac{\partial}{\partial y}\left(VW - K\left(\frac{\partial V}{\partial z} + \frac{\partial W}{\partial y}\right)\right) + \frac{\partial}{\partial z}\left(W^2 - K_a\frac{\partial W}{\partial z}\right) = -\frac{\partial P}{\partial z} - C_d A W\sqrt{U^2 + V^2 + W^2}. \tag{8}$$

The inclusion of the normal stress gradients in Equations (6) to (8) through the Boussinesq eddy-viscosity approximation of Equation (5) does have the purely computational advantage of providing "stabilizing" diffusion terms. For simplicity, we have neglected the normal stress gradients, but to ensure numerical stability, we added diffusion terms in Equations (6) to (8) where diffusion was otherwise absent (through the neglect of the normal stress gradients). We regard these as purely artificial, and signify the artificial diffusivity as K_a, which is very small. Hence, K_a is used for no other purpose than to stabilise the numerical solution of Equations (6) to (8).

The only unspecified quantity in Equations (6) to (8) is the (true) eddy viscosity, K. The latter may always be regarded as the product ($K = \lambda\Gamma$) of a turbulence length scale (λ) and velocity scale (Γ). Its specification, propitious or otherwise, is often the key to the success of a flow simulation. In our case, the eddy viscosity is estimated as

$$K = \lambda(x, y, z)\sqrt{c_e k(x, y, z)}. \tag{9}$$

Here, the turbulence length scale λ is a function of x, y, and z for an inhomogenous urban canopy. In this specification for K, $k^{1/2}$ has been used as the turbulence velocity scale. The constant, c_e, in Equation (9) is the equilibrium shear stress/TKE ratio (u_{*0}^2/k_0) immediately above the canopy. It should be noted that this constant, when evaluated in the local equilibrium region of a free-shear or boundary-layer flow, varies little from one flow configuration to another. In particular, various measurements which have been summarized by Townsend [11] indicate that for boundary layers, wakes, and mixing layers, c_e is nearly the same and varies between about 0.2 to 0.3. The TKE, $k(x, y, z)$, is calculated as a dynamic variable from the following approximate transport equation:

$$\begin{aligned}\frac{\partial}{\partial x}\left(Uk - \mu K\frac{\partial k}{\partial x}\right) + \frac{\partial}{\partial y}\left(Vk - \mu K\frac{\partial k}{\partial y}\right) + \frac{\partial}{\partial z}\left(Wk - \mu K\frac{\partial k}{\partial z}\right) \\ = K\left[\left(\frac{\partial U}{\partial y} + \frac{\partial V}{\partial x}\right)^2 + \left(\frac{\partial U}{\partial z} + \frac{\partial W}{\partial x}\right)^2 + \left(\frac{\partial V}{\partial z} + \frac{\partial W}{\partial y}\right)^2\right] + P_w - \epsilon,\end{aligned} \tag{10}$$

where P_w is the wake production term and ϵ is the viscous dissipation of TKE. The constant μ in Equation (10) represents the ratio of the effective eddy diffusivity for TKE to the eddy viscosity (i.e., inverse of a turbulent Schmidt number). For simplicity, in the basic version of this windflow model, it is assumed that $P_w = 0$. From this simplified perspective, we regard k as excluding the TKE residing in the wake-scales, in which case the gain to k from the mean kinetic energy (MKE) is excluded. The TKE dissipation (i.e., sink $-\epsilon$) in Equation (10) is then specified as $\epsilon = \max(\epsilon_{\rm cc}, \epsilon_{\rm fd})$ where

$$\epsilon_{\rm cc} = \frac{(c_e k)^{3/2}}{\lambda}, \qquad \text{and} \qquad \epsilon_{\rm fd} = \alpha_* C_d A k\sqrt{U^2 + V^2 + W^2}. \tag{11}$$

The term ϵ_{cc} is the standard parameterization for viscous dissipation. the only TKE sink above the canopy (i.e., ϵ_{cc} balances shear production of TKE, in the local equilibrium layer well above the canopy). Our specification for ϵ_{fd} ("form drag"), which converts resolved TKE to the small, rapidly dissipated "wake-scales", can be justified on physical grounds. It is expected that α_* is an order one closure constant, but its exact value depends on the partitioning of k between the three velocity components (u', v', w'). Clearly, the particular canopy geometry plays a role in the energy partition.

It remains to specify the turbulence length scale λ. Ideally, this turbulence length scale should be determined as a dynamic variable for the case of inhomogeneous canopy flows but, for simplicity, we choose instead to specify this quantity algebraically. In this sense, the current windflow model is incomplete since the turbulence length scale is not provided automatically by the model proper, but needs to be specified in terms of some relevant flow characteristics of the canopy. To this purpose, the turbulence length scale is modeled as $\lambda = \max(\lambda_i, \lambda_o)$ where

$$\frac{1}{\lambda_i} = \frac{1}{k_v z} + \frac{1}{\lambda_c} \qquad \text{and} \qquad \frac{1}{\lambda_o} = \frac{1}{k_v (z-d)} + \frac{1}{L_\infty}. \tag{12}$$

The "outer" scale λ_o recognizes the displacement (of the equilibrium structure) due to the canopy (through the zero plane displacement d) and, through the imposed (i.e., maximum permitted) value L_∞, the restricted depth of the PBL. In the case of a full PBL simulation, L_∞ should limit the length scale to the PBL depth which is often estimated [12] as approximately

$$L_\infty = \frac{0.0004 U_G}{f}. \tag{13}$$

The "inner" scale λ_i recognizes both the limitation on eddy size by proximity to the ground and the presence of the canopy. The influence of the canopy on the length scale is embodied in λ_c, the canopy shear length scale which is taken as

$$\lambda_c(x,y) = \frac{c k^{1/2}(x,y,z=h_c)}{\left.\dfrac{\partial S}{\partial z}\right|_{z=h_c}}, \tag{14}$$

where $S \equiv (U^2 + V^2)^{1/2}$ is the horizontal windspeed and c is an order one [viz., $c \sim O(1)$] closure constant. The canopy shear length scale has been shown [13] to play a critical role in the dynamical process that produces the dominant canopy eddies.

The basic windflow model described above has three closure constants that need to be specified; namely, the inverse of the turbulent Schmidt number, μ [Equation (10)]; the coefficient, α_*, specifying the form drag dissipation [Equation (11)]; and, the constant of

proportionality, c, that relates the canopy shear length scale to turbulence velocity scale and mean shear at canopy height [Equation (14)]. If our theory were exact, we could set the values of these coefficients from first principles. Unfortunately, the theory is not exact, but rather a model developed mainly on the strength of dimensional analysis. Consequently, the best we could do is to set the values of the closure coefficients to assure agreement with observed properties of canopy flows. To this purpose, Wilson et al. [14] calibrated the basic windflow model against windflow observations obtained upwind from the ridge in the Furry hillflow experiments [15]. The optimization of the closure constants with respect to the Furry Hill upwind observations yielded the following values for the closure coefficients: $c = 1.0$, $\alpha_* = 1.0$, and $\mu = 0.2$.

In addition to the basic windflow model described above, we will consider also an alternative variant of this model. Although three closure constants have been specified in the basic windflow model by calibrating the closure scheme against the Furry Hill data, in the alternative variant of this model we consider the removal of two of these closure constants. According to Launder and Spalding [16,17], the specification $\mu = 1.0$ (equality of eddy viscosity and eddy diffusivity for TKE or, equivalently, the turbulent Schmidt number for TKE is unity) is optimal for free shear flows (plane jets and mixing layers); and, also for boundary-layer flows, μ should have a value that is approximately unity. In view of the similarity of canopy flows and plane mixing layer flows [13], it is surprising that $\mu = 0.2$ is optimal based on comparison with the Furry Hill upwind observations. It is possible that our specification $\mu = 0.2$ in the basic model is due to deficiencies in our representation of other terms in the transport equation for TKE, particularly in the wake production and form drag dissipation terms. In view of this possibility, in the alternative windflow model, we adopt the standard recommendation that $\mu = 1$ [16,17] and consider more carefully the parameterization of the wake production and form drag dissipation terms.

In the basic windflow model, the wake production term P_w was assumed to be zero (viz., the MKE conversion term is omitted) with the effective gain to the TKE from the MKE and loss from the TKE to smaller dissipative scales being parameterized in terms of a viscous dissipation of the form $\epsilon = \max(\epsilon_{cc}, \epsilon_{fd})$, with the closure constant α_* associated with our rather inelegant representation of the form drag dissipation [cf. Equation (11)]. In view of the solid bluff obstacles comprising an urban canopy, it is reasonable for these obstacles (with characteristic dimensions comparable to the canopy height) to transfer k, not to irrelevant fine-scale wake scales that are rapidly dissipated but, rather, to larger eddies in the energetic sub-range and/or the inertial-convective sub-range that will be involved in a further dyanamical role in the canopy processes. To parameterize the wake production, we make the assumption that the partition of the resulting TKE between velocity components

is isotropic at the wake scales (approximately or better) and write

$$P_{ij}^{w} = C_d A\big(U^2 + V^2 + W^2\big)^{3/2}\frac{\delta_{ij}}{3}, \tag{15}$$

as the wake production contribution to $\overline{u_i' u_j'}$ (creation of $\overline{u_i' u_j'}$ as the mean flow does work against canopy drag). In consequence, the wake production of TKE is

$$P_w = \frac{1}{2}P_{ii}^{w} = \frac{1}{2}C_d A\big(U^2 + V^2 + W^2\big)^{3/2}. \tag{16}$$

In summary, in our alternative windflow model we retain wake production in the form parameterized by Equation (16) as a gain term in the TKE transport equation because urban canopies tend to be dominated by large-scale structures (buildings) with dimensions and separations of the same order as the height of the canopy.

In retaining the wake production term, we consider also a more careful treatment of the process of dissipation of this wake TKE in our alternative windflow model. The form drag dissipation accounts for the conversion of resolvable TKE to heat in the obstacle wakes by working of the turbulent flow against obstacle drag. The instantaneous drag force acting in the i-th coordinate direction can be written as $F_i = -C_d A\|\mathbf{u}\|u_i$ $(i = 1, 2, 3)$, where $\mathbf{u} \equiv (u_1, u_2, u_3) = (U_1 + u_1', U_2 + u_2', U_3 + u_3')$ is the total instantaneous velocity vector and $\|\cdot\|$ denotes the Euclidean norm of a vector. The dissipation of the specific Reynolds stress $\overline{u_i' u_j'}$ due to form drag (which is denoted by $\epsilon_{\mathrm{fd}}^{ij}$) arises from the working of the turbulence against the fluctuating drag force (F_i') and can be obtained from the following expression:

$$\begin{aligned}\epsilon_{\mathrm{fd}}^{ij} &= \overline{u_i' F_j'} + \overline{u_j' F_i'} \\ &= C_d A\Big(U_j\overline{\|\mathbf{U}\|u_i'} + U_i\overline{\|\mathbf{U}\|u_j'} + 2\overline{\|\mathbf{U}\|u_i' u_j'}\Big).\end{aligned} \tag{17}$$

Now, note that the Euclidean norms of the total instantaneous velocity vector, the mean velocity vector, and the fluctuating velocity vector are related as $\|\mathbf{u}\| = \|\mathbf{U}\| + \|\mathbf{u}'\|$. Inserting this relationship in Equation (17) and neglecting all terms involving third-order moments of the velocity fluctuations, we obtain the following approximate expression for $\epsilon_{\mathrm{fd}}^{ij}$:

$$\epsilon_{\mathrm{fd}}^{ij} \approx C_d A\Big(U_j\overline{\|\mathbf{u}'\|u_i'} + U_i\overline{\|\mathbf{u}'\|u_j'} + 2\|\mathbf{U}\|\overline{u_i' u_j'}\Big). \tag{18}$$

As it currently stands, Equation (18) cannot be used in our alternative windflow model because we need some method to estimate the correlation $\overline{\|\mathbf{u}'\|u_i'}$. To this purpose, we first observe that $\|\mathbf{u}'\|u_i'$ can be expressed as

$$\|\mathbf{u}'\|u_i' = \left[\|\mathbf{U}\|\left(1 + \frac{2U_k u_k'}{\|\mathbf{U}\|^2} + \frac{u_k' u_k'}{\|\mathbf{U}\|^2}\right)^{1/2} - \|\mathbf{U}\|\right]u_i'. \tag{19}$$

Now apply a binomial series expansion to the square root term in Equation (19) and ensemble-average the resulting expression, neglecting all terms involving velocity moments higher than second-order, to get

$$\overline{\|\mathbf{u}'\|u_i'} \approx \frac{U_k \overline{u_k' u_i'}}{\|\mathbf{U}\|}. \tag{20}$$

Finally, inserting Equation (20) into Equation (18) gives the following practical estimate for $\epsilon_{\mathrm{fd}}^{ij}$:

$$\epsilon_{\mathrm{fd}}^{ij} \approx C_d A \left(2\|\mathbf{U}\|\overline{u_i' u_j'} + U_j U_k \frac{\overline{u_k' u_i'}}{\|\mathbf{U}\|} + U_i U_k \frac{\overline{u_k' u_j'}}{\|\mathbf{U}\|} \right). \tag{21}$$

In view of Equation (21), the form drag dissipation of TKE can be obtained from

$$\epsilon_{\mathrm{fd}} = \frac{1}{2}\epsilon_{\mathrm{fd}}^{ii} = C_d A \left(2\|\mathbf{U}\|k + U_i U_k \frac{\overline{u_k' u_i'}}{\|\mathbf{U}\|} \right). \tag{22}$$

The parameterization for ϵ_{fd} in Equation (22) [which we use in the alternative windflow model] does not involve any closure constants, in contrast to the parameterization of Equation (11) used in the basic windflow model.

In summary, the alternative windflow model eliminates two closure constants used in the basic windflow model. Firstly, the turbulent Schmidt number μ^{-1} is set exactly to unity, which is consistent with others' shear layer simulations where the eddy viscosity is assumed to be identical to the turbulent diffusivity for TKE. Secondly, Equation (22) is used as the parameterization for the form drag dissipation ϵ_{fd}, eliminating the closure constant α_*. The remaining closure constant c (which arises as the proportionality constant in specification of the canopy shear length scale) retains the same value that it has in the basic windflow model (namely, $c = 1$).

This page intentionally left blank

Experimental data for model evaluation

The ideal way to assess the accuracy of the basic and alternative canopy windflow models is to compare their performances for a broad range of canopy test flows. We restrict our attention to experiments providing measurements of both the mean flow and the turbulence (shear stress, TKE, and/or normal stresses), and depend heavily on data from controlled experiments in a wind tunnel or water channel. A number of vegetative and urban canopies has been chosen for this model evaluation, but the emphasis has been placed on canopies composed of solid bluff obstacles (i.e., "urban" canopies). The canopies considered here are uniform. In an ideal assessment of the accuracy of a model, extraneous errors (e.g., measurement error, numerical error, discrepancies in the boundary conditions, etc.) need to be shown to be small so that the discrepancy between measured and calculated flow properties arise only from inaccuracies of the model (i.e., model error); the test flows should be different than those used in the development of the model; and, the tests should not be performed by the model's developers. Even though the model evaluation reported here does not conform to this ideal in all respects, it is nevertheless hoped that the results are useful in helping the reader assess the accuracy and utility of the proposed canopy windflow models.

For each experiment, we determined a bulk drag coefficient, C_d, using the information from the measured mean wind and shear stress within the canopy. To this end, C_d was determined from

$$\frac{\tau(h_c)}{u_{*0}^2} \equiv C_d A h_c \int_0^1 \left(\frac{U}{u_{*0}}\right)^2 d\frac{z}{h_c}, \tag{23}$$

where $\tau(h_c)$ is the shear stress at the canopy top ($z = h_c$) [i.e., $\tau \equiv -\overline{u'w'}$] and u_{*0} is the reference friction velocity derived from the shear stress at canopy top. In writing Equation (23), we have explicitly assumed that the canopy is uniform. Furthermore, in our model simulations as well as in the presentation of the experimental data, u_{*0} is used as the reference velocity scale for the normalization of all flow quantities. From observations of σ_u, σ_v, and σ_w (standard deviations of velocity fluctuations in the streamwise, cross-stream, and vertical directions, respectively) above the canopy, we determined equilibrium ratios $c_u \equiv \sigma_u/u_{*0}$, $c_v \equiv \sigma_v/u_{*0}$ and $c_w \equiv \sigma_w/u_{*0}$ and

$$c_e = \frac{2}{c_u^2 + c_v^2 + c_w^2}. \tag{24}$$

For the canopy flows in wind tunnel and water channel experiments, there was a vertical gradient in the shear stress above the canopy (balanced by advection). Normally, in these kinds of experiments the inertial sublayer, where the shear stress is constant and where the

mean velocity adheres to the logarithmic law-of-the-wall profile, is "squeezed" out between the roughness sublayer and outer layer owing to the large value of h_c/δ (where δ is the boundary-layer depth) compared with the atmosphere. In consequence, in order to properly account for stress and TKE gradients at $z > h_c$ in the canopy flow experiments conducted in a wind tunnel or water channel, we incorporated an effective background kinematic pressure gradient which was assigned from the measured shear stress gradient above the canopy, viz.

$$\frac{1}{u_{*0}^2}\frac{\partial P_e}{\partial x/h_c} = \frac{\partial}{\partial z/h_c}\left(\frac{\tau}{u_{*0}^2}\right) \qquad z > h_c, \tag{25}$$

where P_e is the effective kinematic pressure. The value for the effective kinematic pressure gradient, determined in Equation (25) for the experiment, was imposed in the simulations of the experiment. The canopies used in this model evaluation are described briefly below. The first two canopies are vegetative canopies composed of flexible elements; the remaining nine canopies correspond to urban canopies composed of solid bluff obstacles.

Brunet et al. [18] described a wind tunnel "wheat" canopy in detail that consisted of an array of stalks constructed from monofilament nylon fishing line of diameter 0.25 mm, spaced on a uniform square grid of side 5 mm. Each stalk was nominally 50 mm long but, because of the natural tendency of the stalk to bend, the mean canopy height h_c was only 47 mm. In the Furry Hill experiment [19], this canopy was placed upwind and over a Witch of Agnesi ridge. The parameters of this canopy, relevant for the present work, are summarized in Table 1. For the specification of σ_v (which was not measured) and the TKE, the approximation that $\sigma_u = \sigma_v$ was used.

Table 1. *Parameters of the Furry Hill experiment.*

Property	Symbol	Value
Canopy height	h_c	0.047 m
Bulk drag parameter	$C_d A h_c$	0.32
Frontal area per unit volume	A	10.0 m^{-1}
Friction velocity	u_{*0}	0.975 m s^{-1}
Mean wind at $z = h_c$	$U(h_c)/u_{*0}$	3.7
Equilibrium standard deviations	$(\sigma_u, \sigma_v, \sigma_w)/u_{*0}$	2.2, 2.2, 1.25
TKE at $z = h_c$	$k(h_c)/u_{*0}^2$	5.62
Effective pressure gradient	$(h_c/u_{*0}^2)\partial P_e/\partial x$	−0.16
Displacement height	d	0.0333 m

The Elora corn canopy was described by Wilson et al. [20] who presented profiles of mean wind and turbulence statistics within (but not above) a mature corn canopy at Elora,

Ontario. The measurements of the flow statistics were made using servo-controlled, split-film, heat-transfer anemometers. Some relevant parameters for this canopy are presented in Table 2. A deep constant stress layer was used as the background flow for this simulation.

Table 2. *Parameters of the Elora corn canopy experiment.*

Property	Symbol	Value
Canopy height	h_c	2.21 m
Bulk drag parameter	$C_d A h_c$	0.79
Mean wind at $z = h_c$	$U(h_c)/u_{*0}$	3.04
Equilibrium standard deviations	$(\sigma_u, \sigma_v, \sigma_w)/u_{*0}$	2.06, 1.65, 1.13
TKE at $z = h_c$	$k(h_c)/u_{*0}^2$	4.12
Displacement height	d	1.5 m

Macdonald et al. [21] reported profiles of mean wind and turbulence statistics in square arrays of cubical obstacles with frontal area indices λ_F (frontal area of obstacle normalized by the lot area within which a single obstacle sits) of 0.0625, 0.16, and 0.44 corresponding, respectively, to isolated roughness flow, wake interference flow, and skimming flow. In these square (in-line) arrays, there were unobstructed streets between the obstacles in the direction of the approaching wind. These experiments were conducted in a water channel using a SonTek MicroADV acoustic Doppler velocimeter to measure the flow velocities. The parameters for these square arrays are given in Table 3. In all these obstacles arrays, the frontal area density A can be determined from $A = \lambda_F/h_c$.

Macdonald et al. [21] provided data on mean wind and turbulence within and above staggered arrays of cubical obstacles with frontal area indices $\lambda_F = 0.0625$, 0.16, and 0.44. In these uniform obstacles arrays, alternate rows of obstacles (cubes) were shifted by half the center-to-center spacing between the obstacles. For the staggered arrays of cubes with $\lambda_F = 0.0625$, 0.16, and 0.44, the parameters relevant to the model simulations can be summarized in Table 4.

The last set of obstacle arrays selected are square and staggered arrays of billboard-shaped obstacles. Unlike cubical obstacles, the billboard-shaped obstacles have small depth with the result that the obstacles are effectively two-dimensional (approximately or better). Macdonald et al. [21] measured the mean wind and turbulence statistics within and above square and staggered arrays of billboard-shaped obstacles with a frontal area index $\lambda_F = 0.16$. The obstacles, machined from aluminum angle sections, were 50 mm wide, 3 mm thick, and 50 mm high. The relevant parameters for the square and staggered arrays of obstacles are

given in Table 5.

Table 3. *Parameters of the square arrays of cubical obstacle experiments.*

Property	Symbol	Value
	Frontal area density $\lambda_F = 0.0625$	
Canopy height	h_c	0.05 m
Bulk drag parameter	$C_d A h_c$	0.025
Friction velocity	u_{*0}	0.0048 m s^{-1}
Mean wind at $z = h_c$	$U(h_c)/u_{*0}$	8.8
Equilibrium standard deviations	$(\sigma_u, \sigma_v, \sigma_w)/u_{*0}$	2.1, 1.6, 1.2
TKE at $z = h_c$	$k(h_c)/u_{*0}^2$	3.78
Effective pressure gradient	$(h_c/u_{*0}^2)\partial P_e/\partial x$	-0.16
	Frontal area density $\lambda_F = 0.16$	
Canopy height	h_c	0.05 m
Bulk drag parameter	$C_d A h_c$	0.078
Friction velocity	u_{*0}	0.0051 m s^{-1}
Mean wind at $z = h_c$	$U(h_c)/u_{*0}$	6.2
Equilibrium standard deviations	$(\sigma_u, \sigma_v, \sigma_w)/u_{*0}$	2.1, 1.7, 1.2
TKE at $z = h_c$	$k(h_c)/u_{*0}^2$	3.63
Effective pressure gradient	$(h_c/u_{*0}^2)\partial P_e/\partial x$	-0.22
	Frontal area density $\lambda_F = 0.44$	
Canopy height	h_c	0.05 m
Bulk drag parameter	$C_d A h_c$	0.24
Friction velocity	u_{*0}	0.0025 m s^{-1}
Mean wind at $z = h_c$	$U(h_c)/u_{*0}$	5.14
Equilibrium standard deviations	$(\sigma_u, \sigma_v, \sigma_w)/u_{*0}$	2.1, 1.7, 1.2
TKE at $z = h_c$	$k(h_c)/u_{*0}^2$	4.96
Effective pressure gradient	$(h_c/u_{*0}^2)\partial P_e/\partial x$	-0.17

Raupach et al. [22] reported profiles of mean wind and turbulence statistics in the Tombstone canopy which was an array of vertical bars (flat plates) 60 mm high, 10 mm wide, and 1 mm thick arranged in a staggered (diamond) pattern with 60 mm cross-stream and 44 mm streamwise spacing. This obstacle arrangement resulted in a frontal area index of 0.23. Velocity statistics were measured with a specially developed 3-wire probe [23] in a wind tunnel. The parameters that characterize this canopy are summarized in Table 6. Because only two components of the instantaneous velocity (namely, u and w) were measured in this experiment, the cross-stream velocity standard deviation σ_v and the TKE k were obtained

assuming that $\sigma_v^2 = \sigma_u \sigma_w$ (viz., the cross-stream standard deviation of velocity fluctuations is the geometric mean of the streamwise and vertical velocity fluctuations).

Table 4. *Parameters of the staggered arrays of cubical obstacle experiments.*

Property	Symbol	Value
	Frontal area density $\lambda_F = 0.0625$	
Canopy height	h_c	0.05 m
Bulk drag parameter	$C_d A h_c$	0.042
Friction velocity	u_{*0}	0.0053 m s^{-1}
Mean wind at $z = h_c$	$U(h_c)/u_{*0}$	7.2
Equilibrium standard deviations	$(\sigma_u, \sigma_v, \sigma_w)/u_{*0}$	2.0, 1.6, 1.2
TKE at $z = h_c$	$k(h_c)/u_{*0}^2$	3.49
Effective pressure gradient	$(h_c/u_{*0}^2)\partial P_e/\partial x$	-0.16
	Frontal area density $\lambda_F = 0.16$	
Canopy height	h_c	0.05 m
Bulk drag parameter	$C_d A h_c$	0.11
Friction velocity	u_{*0}	0.0062 m s^{-1}
Mean wind at $z = h_c$	$U(h_c)/u_{*0}$	4.9
Equilibrium standard deviations	$(\sigma_u, \sigma_v, \sigma_w)/u_{*0}$	2.0, 1.6, 1.2
TKE at $z = h_c$	$k(h_c)/u_{*0}^2$	2.94
Effective pressure gradient	$(h_c/u_{*0}^2)\partial P_e/\partial x$	-0.24
	Frontal area density $\lambda_F = 0.44$	
Canopy height	h_c	0.05 m
Bulk drag parameter	$C_d A h_c$	0.31
Friction velocity	u_{*0}	0.0026 m s^{-1}
Mean wind at $z = h_c$	$U(h_c)/u_{*0}$	5.4
Equilibrium standard deviations	$(\sigma_u, \sigma_v, \sigma_w)/u_{*0}$	2.2, 1.7, 1.2
TKE at $z = h_c$	$k(h_c)/u_{*0}^2$	6.16
Effective pressure gradient	$(h_c/u_{*0}^2)\partial P_e/\partial x$	-0.14

Table 5. *Parameters of the square and staggered arrays of billboard obstacle experiments for frontal area density,* $\lambda_F = 0.16$.

Property	Symbol	Value
	Square Array	
Canopy height	h_c	0.05 m
Bulk drag parameter	$C_d A h_c$	0.35
Friction velocity	u_{*0}	0.0082 m s^{-1}
Mean wind at $z = h_c$	$U(h_c)/u_{*0}$	3.4
Equilibrium standard deviations	$(\sigma_u, \sigma_v, \sigma_w)/u_{*0}$	2.0, 1.6, 1.2
TKE at $z = h_c$	$k(h_c)/u_{*0}^2$	3.40
Effective pressure gradient	$(h_c/u_{*0}^2)\partial P_e/\partial x$	−0.22
	Staggered Array	
Canopy height	h_c	0.05 m
Bulk drag parameter	$C_d A h_c$	0.23
Friction velocity	u_{*0}	0.0080 m s^{-1}
Mean wind at $z = h_c$	$U(h_c)/u_{*0}$	3.2
Equilibrium standard deviations	$(\sigma_u, \sigma_v, \sigma_w)/u_{*0}$	1.9, 1.5, 1.2
TKE at $z = h_c$	$k(h_c)/u_{*0}^2$	3.13
Effective pressure gradient	$(h_c/u_{*0}^2)\partial P_e/\partial x$	−0.24

Table 6. *Parameters of the Tombstone canopy experiment.*

Property	Symbol	Value
Canopy height	h_c	0.06 m
Bulk drag parameter	$C_d A h_c$	0.31
Friction velocity	u_{*0}	1.1 m s^{-1}
Mean wind at $z = h_c$	$U(h_c)/u_{*0}$	3.09
Equilibrium standard deviations	$(\sigma_u, \sigma_v, \sigma_w)/u_{*0}$	2.0, 1.5, 1.14
TKE at $z = h_c$	$k(h_c)/u_{*0}^2$	3.8
Effective pressure gradient	$(h_c/u_{*0}^2)\partial P_e/\partial x$	−0.23

Model comparisons

The numerical method used as the basis for this work is described in detail in [10]. Briefly, the governing fluid equations for both the basic and alternative canopy windflow models were solved using a finite-volume discretization along with a staggered grid arrangement. Over this grid system, the governing fluid flow equations are discretized and this yields a set of equivalent discrete algebraic equations. These algebraic equations are then solved by an iterative procedure, subject to the appropriate boundary conditions which specify the problem. The SIMPLEC algorithm [24] was used to couple pressure and velocity on the staggered grid, and a line-by-line iterative procedure was applied to solve the discretized system of algebraic equations over the computational domain. Because all the model simulations involved uniform canopies, horizontal homogeneity is assumed leading to $\partial/\partial x_i = 0$ for $i = 1, 2$. All the simulations are done in rotated coordinates so that the flow is in the x_1-direction (i.e., $V \equiv 0$).

Local equilibrium lower boundary conditions are used for U and k. In the staggered grid that defines abutting control volumes for U and k, we have set the lowest TKE gridpoints on the ground. Consequently, the lowest U gridpoints lie above the ground and a "wall function" relationship is used to relate the surface shear-stress and the near-ground windspeed. In particular, if the lowest U gridpoints lie at $z = z_P$, then a condition on the corresponding vertical momentum fluxes to ground is required. In other words, the boundary condition on U (tangential component of $\mathbf{U}$) is applied implicitly through the specification of the shear stress as $\overline{u'w'} = -u_*^2$ where

$$u_* = \kappa U_P / \ln\left(\frac{z_P}{z_{0s}}\right). \tag{26}$$

Here, $\kappa \approx 0.4$ is von Karman's constant, $U_P \equiv U(z_P)$, and z_{0s} is the substrate roughness length at the ground. In practice, the value of z_{0s} is chosen rather arbitrarily, with simulations showing very little sensitivity to a wide range of values. All the model simulations presented in the reported used $z_{0s} = 0.00001$ m. The imposition of this lower boundary condition is consistent with a constant stress, logarithmic mean profile at the lower boundary (ground), which is the simplest consistent assumption that we can make about conditions at the ground surface below the canopy. Of course, strictly speaking, these wall relationships are not valid within the canopy (nor for that matter in regions of highly-disturbed flow), but as the shear stress on the ground beneath a canopy (that is not too sparse) is generally small, its miscalculation (by the above relationships) is expected to carry negligible penalty. As the lower boundary condition on TKE in conjunction with Equation (26), we adopted the equilibrium relationship $k_{\text{gnd}} = u_*^2/c_e$. The alternative prescription $(\partial k/\partial z)_{z=0} = 0$

performed neither better nor worse.

We set the uppermost U gridpoint in a normal, full, control volume, bounded by the top of the computational domain, so that the upper-boundary condition on U was a specified shear stress. Either we specified this shear stress aloft as undisturbed (u_{*0}^2) and constituting the velocity scale for the simulation (in the case of a field simulation such as the Elora corn canopy); or, to properly account for stress and TKE gradients at $z > h_c$ in the incident flow, we incorporated an effective background kinematic pressure gradient [cf. Equation (25)], and specified the shear stress aloft as $-\overline{u'w'}(z = z_T) = u_{*0}^2 + \frac{\partial P_e}{\partial z}(z_T - h_c)$, where z_T is the top of the computational domain and $\partial P_e/\partial z = (\partial \tau/\partial z)$ is the measured stress gradient above the canopy (in the case of a wind tunnel or water channel simulation). Since a k gridpoint lies on the upper boundary of the computational domain, we applied the Neumann boundary condition $(\partial k/\partial z)_{z=z_T} = 0$. This is not quite correct for the wind tunnel or water channel simulations because of the TKE gradients above the canopy, but the alternative of specifying the value of k directly at the top of the computational domain required an *a priori* knowledge of this value (which we assume would not be available generally). In all our model simulations, we "turned off" the Coriolis acceleration by setting $f = 0$ because the full PBL was not required.

Other rather familiar parameters have appeared in our canopy windflow model equations, as constants which we want to clearly distinguish from the closure parameters—to emphasize that the success of our simulations does not depend on any flexibility in their specification. They are L_∞, d, and c_e and are determined by the flow properties taken from within the constant stress layer above the canopy. Firstly, the turbulence length scale [cf. Equation (12)] requires the assignment of L_∞ which imposes a limiting value on the magnitude of the outer length scale. For a full PBL simulation, L_∞ is assigned using Equation (13). However, for numerical simulations of the wind tunnel and water channel data, we set $L_\infty/h_c = 1.0$ to accomodate the shallowness of the above-canopy constant-stress layer in these flows. For the field experiments (e.g., Elora corn canopy), we assumed a deep constant-stress layer for the background flow and set $L_\infty = \infty$. The numerical value of L_∞ affects our simulated profiles of U, τ, and k only far above the canopy in a region of little interest to us. The aim was not to replicate the actual details of the flow aloft (which for the wind tunnel and water channel simulations would depend on actual mechanisms [e.g., boundary-layer trips, spires, upstream roughness elements] used to accelerate the development of the boundary-layer above the canopy), but merely to ensure that the modeling of the disturbed flow through the canopy (which is the region of greatest interest in this study) was not compromised by an inherently unrealistic treatment aloft. Secondly, the displacement length d required in the definition of the outer turbulence length scale λ_o [cf. Equation (12)] was either assigned

the value reported for the canopy (e.g., Furry Hill and Elora corn canopy simulations), or estimated using a similarity relationship for d in regular obstacle arrays proposed by Macdonald et al. [25] (e.g., for the wind tunnel and water channel "urban" canopy simulations). Thirdly, the value of c_e [cf. Equation (11)] was determined for each canopy from the measurements of the equilibrium ratios $c_u = \sigma_u/u_{*0}$, etc. above the canopy [cf. Equation (24)]. However, these equilibrium ratios in flows above uniform canopies typically vary little from one canopy to the next. Indeed, typically $\sigma_{u,v,w}/u_{*0} \approx 2.1, 1.7, 1.2$, implying $c_e \approx 0.23$. This value for c_e could have been used for all the model simulations, with little change in the final results.

It only remained in the model simulations to specify the bulk drag coefficient C_d (note that A and h_c are determined from the geometric characteristics of the canopy). Unfortunately, there exists currently no theory that allows one to predict the bulk drag coefficient of a canopy from knowledge of the canopy geometry and the behavior of the obstacle elements in isolation. In our canopy windflow model, we view C_d as a data input. For model evaluation, the value of C_d for a particular canopy was diagnosed from the measurements of the mean wind and shear stress within the canopy [cf. Equation (23)]. This is in contrast to the alternative of considering C_d as an adjustable model parameter whose value is simply adjusted to optimise the fit between modeled and measured mean profiles. The first approach ensures that the "true" rate of momentum extraction occurs within the canopy regardless of the wind speed.

The canopy windflow model used in this study is a one-equation model that is based on an approximate transport equation for the turbulence kinetic energy and on the use of the Boussinesq linear eddy-viscosity approximation to compute the Reynolds stress tensor as the product of an eddy viscosity and the mean strain-rate tensor. As a further approximation, we assumed that the normal stress gradients play a much smaller role than the shear stress gradients in the determination of the mean flow, so we neglected the normal stress gradient contributions to the mean momentum equations, replacing them instead with small artificial diffusion terms. These diffusion terms were added simply to ensure numerical stability. The artificial viscosity K_a used to characterize these diffusion terms is very small. Generally, for the current model simulations, the artificial viscosity was specified as $K_a = 0.01 h_c u_{*0}$ and had insignificant effect on the simulations other than to ensure numerical stability. For model comparisons, the velocity variances (normal stresses) σ_u^2, σ_v^2, and σ_w^2 were derived from the calculated TKE, assuming equilibrium partitioning, i.e. $\sigma_u^2 = c_e c_u^2 k$, $\sigma_v^2 = c_e c_v^2 k$, and $\sigma_w^2 = c_e c_w^2 k$. Note that this reduces to the special instance of isotropic partitioning of the TKE if and only if $c_u = c_v = c_w$, which is generally not the case for canopy flows.

Figures 1, 2, and 3 compare modeled and measured profiles of U, τ, and k for the aeroelastic plant canopy used in the Furry Hill experiment. In this and subsequent comparisons, the solid and long dashed curves correspond to predictions obtained from the basic and alternative canopy windflow models, respectively. Vertical axes are scaled by h_c, while mean velocity and turbulence profiles are scaled by u_{*0} and u_{*0}^2, respectively. The basic windflow model (viz., simulations using $c = \alpha_* = 1$, $\mu = 0.2$; all other inputs [d, c_e, C_d, A] provided unambiguously by the Furry Hill observations) provides excellent agreement with the Furry Hill data, although it must be emphasized that the closure constants here were optimized with respect to this data set. The quantitative agreement between model and observations for the alternative windflow model (viz., $c = \mu = 1$ with a model [cf. Equation (22)] for the form drag sink in the TKE transport equation that does not involve the closure constant α_*) is not as good as that for the basic windflow model, but then again the closure constants in the alternative model have not been optimized with respect to the Furry hill data.

The better agreement of the basic model predictions and the Furry Hill observations relative to the alternative model predictions arises primarily from the specification $\mu = 0.2$. Recall that the turbulent diffusivity $K_k = \mu K$ of TKE parameterizes the sum $(T_t + T_p)$ of turbulent (T_t) and pressure (T_p) transport of TKE. Also, recall that on theoretical grounds, Lumley [26] suggested (p' is the kinematic pressure fluctuations)

$$\overline{p'u_j'} \approx -0.2\overline{u_j'u_k'u_k'}.$$

Direct numerical simulations conducted by Rogers and Moser [27] for a plane mixing layer supported Lumley's suggestion. The crucial point is that, if $|T_t + T_p|/|T_t|$ is systematically different in the canopy than in the plane mixing layer, then there is no reason why the conventional specification $\mu = 1$ (as recommended in [16,17]) should obtain. However, the evidence seems to suggest the contrary. Raupach et al [13] showed that the plane mixing layer flow is a useful archetype for turbulence in the vicinity of a canopy, and used this plane mixing layer analogy to provide a "universal" view of canopy turbulence that appears to be consistent over a wide range of canopies. Furthermore, the TKE balance with $\mu = 0.2$ results in a smaller turbulent transport term than Brunet et al [15] observed (viz., the specification $\mu = 0.2$, which implies that a larger fraction of T_t than 20% is negated by T_p in the canopy [contrary to Lumley's suggestion], is not consistent with these measurements of the turbulent transport term). However, the specification $\mu = 0.2$ was kept in the basic windflow model simply because this specification resulted in a better match to the observed $k(z)$ profile in the Furry Hill experiment.

Figures 4, 5, and 6 display basic and alternative canopy model predictions of U, τ, and k, respectively, for the Elora corn canopy. Both the basic and alternative models provide

reasonably good simulations of the field measurements. The alternative model provides a slightly better agreement for the mean velocity profile than the basic model, with the converse being true for the turbulence profiles. For this canopy, the use of a local drag coefficient diagnosed from the measured mean wind and shear stress within the canopy as

$$C_d(z)A(z)h_c = \frac{1}{U^2(z)}\frac{\partial \tau}{\partial z}$$

resulted in a better agreement of model and observations (for both the basic and alternative models), but because such detailed information on the local drag coefficient $C_d(z)$ would usually be unavailable, we have not pursued this approach any further and have performed all simulations using a bulk drag coefficient C_d. With this understanding, it is expected that the model simulations will represent a less perfect reproduction of the data than could be achieved, but this is an accepted cost of keeping the system simple.

Figures 7 and 8 show comparisons of model predictions and observations of the mean velocity (U) and turbulence (τ, k, σ_u^2) for a square array of cubical obstacles with a frontal area index of 0.0625. Both the basic and alternative models are seen to provide very good predictions for the mean velocity U and shear stress τ for this canopy. However, it is observed that the basic model underestimates k and σ_u^2 deep in the canopy. The alternative model, on the other hand, provides a much better estimate of k and σ_u^2 within the canopy. Fortunately, despite the fact that the basic model underestimates k within the canopy, its predictions for U and τ are basically as good as those of the alternative model. This is because the eddy viscosity is proportional to $k^{1/2}$, rendering U and τ remarkably insensitive to wide variations in the treatment of k.

The measured and modeled mean wind and turbulence profiles for the water channel square array of cubical obstacles with a frontal area index of 0.16 are displayed in Figures 9, 10, and 11. The overall conformance of model and observations for the basic and alternative canopy models is similar to that for the square cubical array with $\lambda_F = 0.0625$. It is apparent from Figures 10 and 11 that the equilibrium partitioning of TKE to derive the three turbulent velocity variances σ_u^2, σ_v^2, and σ_w^2 seems to work well for this example. The equilibrium partitioning of k used here for all vertical levels z followed the measured pattern of the partioning of k at the canopy top (which has been summarized in Table 3 under the property of equilibrium standard deviations). Indeed, the magnitude of the three velocity variances is seen to compare favorably with the observations. In addition, it is noted that because the turbulent velocity variances are constructed essentially by applying scaling factors to the associated model profile for k (with the scaling factors determined from the values of c_e, c_u, c_v, and c_w diagnosed from the flow properties above the canopy), all these

profiles have necessarily the same shape. Unfortunately, given the scatter in the turbulence data for this example, it cannot be determined how accurate this shape assumption is.

Next, we consider the comparison of model results with observations of U, τ, k, and σ_u^2 exhibited in Figures 12 and 13 for the square array of cubical obstacles with a frontal area index of 0.44. Although both the basic and alternative windflow models agree with measurements of U within the canopy ($z \leq h_c$), its overall conformance with the observed U profile above the canopy is poor. In particular, both models underpredict severely the magnitude of the mean wind shear at the top of the canopy, and this underprediction leads to the poor agreement of modeled and observed U above the canopy. This case corresponds to the skimming flow regime where the flow in the canopy is vertically-decoupled from the flow aloft, and the windflow models used here do not seem to handle this case well (at least with respect to the prediction of the mean velocity profiles). However, despite this deficiency in our model predictions, overall agreement of predictions with the turbulence profiles (e.g., shear stress, normal stresses, and TKE) is very good. Interestingly, the alternative windflow model (which provides a relatively good prediction of the turbulence level within the square array of cubical obstacles over the range of frontal area indices considered) predicts that the Reynolds stresses (and, the TKE which is simply the trace of the Reynolds stress tensor) diminish from the top of the canopy downwards exponentially for $\lambda_F = 0.44$ (cf. Figures 12 and 13), whereas this rate of decrease is roughly linear for the smaller frontal area densities (cf. Figures 7 to 11 for $\lambda_F = 0.0625$ and 0.16). The data appear to be consistent with this model prediction, although measurements deep within the square cube array with $\lambda_F = 0.44$ are not available for the full confirmation of this prediction owing to measurement constraints imposed by the small separation between the obstacles for this case.

Figures 14, 15, and 16 compare the modeled (obtained from the basic and alternative canopy windflow models) and measured vertical profiles of U, τ, k, σ_u^2, σ_v^2, and σ_w^2 for the staggered array of cubical obstacles with a frontal area index of $\lambda_F = 0.0625$. Similarly, the measured and modeled mean wind and turbulence profiles for the staggered array of cubical obstacles with a frontal area density of 0.16 are shown in Figures 17, 18, and 19. Finally, Figures 20, 21, and 22 compare the mean wind and turbulence profiles with solutions from the basic and alternative windflow models for the staggered array of cubical obstacles with $\lambda_F = 0.44$. On examination of these figures, it is apparent that the overall conformance of model predictions and observations for the staggered cube arrays is similar to that for the corresponding square cube arrays.

Figures 23, 24, and 25 show vertical profiles of mean wind speed (U) and turbulence (τ, k,

σ_u^2, σ_v^2, σ_w^2) for the square array of billboard-shaped obstacles with a frontal area density of 0.16. Numerical simulations obtained from the basic and alternative canopy windflow models are compared with the experimental data. Figure 24 shows reasonable agreement between the modeled and observed profiles for U and τ. However, unlike the cases for the square and staggered arrays of cubical obstacles, the TKE and the turbulent velocity variances within the canopy are seen to be underpredicted by both the basic and alternative windflow models. Unlike the square cube array with $\lambda_F = 0.16$, the square billboard array with the same frontal area index possesses a much smaller plan area density. This implies that the square billboard array posseses much more "free-air" space and, hence, experiences a greater exposure to the wind than the square cube array. A pecularity of the flow over the billboard canopy is that the wind profile aloft is more nearly logarithmic in z than in $z - d$; viz., the displacement length $d \approx 0$, which is consistent with predictions from a similarity relation for d (e.g., Macdonald et al. [25]). In view of the amount of "free-air" space within the billboard canopy, it would seem that a reasonable procedure here would be to eliminate the form-drag sink term contribution in the TKE transport equation (i.e., set $\epsilon_{\rm fd} = 0$ and model the viscous dissipation as $\epsilon = \max(\epsilon_{\rm cc}, \epsilon_{\rm fd}) = \epsilon_{\rm cc}$). Figures 24 shows that eliminating the form drag sink for the TKE (in the alternative windflow model) increases k within the billboard canopy (short dashed curve) to a level that is more representative of the observations, with the concomitant improvement in simulation of the turbulent velocity variances (cf. Figures 24 and 25). Again, it should be noted that these different variations in the treatment of k have little effect on the predictions of U and τ.

The measured and modeled mean wind and turbulence profiles for the staggered array of billboard-shaped obstacles with a frontal area index of 0.16 are displayed in Figures 26, 27, and 28. Again, it is seen that the elimination of the form drag sink in the TKE transport equation provides a better simulation of the turbulence levels (e.g., k, σ_u^2, σ_v^2, and σ_w^2) within a billboard-shaped obstacle canopy. Given the scatter in the measurements of the turbulence profiles, it is seen that equilibrium partitioning of the TKE provides a reasonably good reproduction of the three normal stresses.

Finally, Figures 29, 30, and 31 show observed profiles of U, τ, and k, respectively, for the Tombstone canopy in comparison with numerical simulations using the basic and alternative windflow models as well as a modification of the alternative windflow model with the TKE form drag sink term removed. The model profiles for U and τ are rather good. However, unlike the preceding staggered billboard canopy, the model prediction for k with the form drag sink in the TKE eliminated now overestimates k within the Tombstone canopy. In this case, the alternative windflow model (with the form drag term retained in the TKE transport equation) provides the best conformance with the observations of k. This is suprising in view

of the preceding results for the staggered billboard canopy. This is because the Tombstone canopy studied by Raupach et al. [22] is essentially a staggered array of billboard-shaped obstacles with frontal area density 0.23 and, hence, is very similar to the staggered billboard array with $\lambda_F = 0.16$ investigated by Macdonald et al. [21]. In particular, both these obstacle arrays correspond to near maximally rough flow (i.e., the roughness length z_0 achieves a maximum with frontal area densities $\lambda_F \approx 0.15$–0.2), with the relationships between velocity statistics being very similar: the normalized mean wind speed at canopy top, $U(h_c)/u_{*0} = 3.1$ for the Tombstone canopy compared with $U(h_c)/u_{*0} = 3.2$ for the billboard canopy; and, the normalized TKE at canopy height, $k(h_c)/u_{*0}^2 = 3.8$ for the Tombstone canopy which is close to the value $k(h_c)/u_{*0}^2 = 3.2$ for the billboard canopy. However, despite these similarities, it is seen that the measured TKE within the Tombstone canopy is systematically smaller in value than that observed in the staggered billboard canopy. Furthermore, the TKE diminishes roughly linearly within the staggered billboard canopy (cf. Figure 27), whereas the TKE in the Tombstone canopy exhibits a nonlinear decrease (i.e., exponential-like decrease) within the canopy. It is unknown whether these seemingly differing estimates of the TKE in these two rather similar canopies is the result of measurement error or is a physical effect arising from the slight differences in the two canopies.

Discussion and conclusions

The basic and alternative canopy windflow models were applied to simulate flows in a wide range of canopies (both vegetative and urban). The models were assessed by comparison with available wind tunnel, water channel, and field data, where we have restricted our attention to experiments providing measurements of both the mean flow and the turbulence (shear stress, TKE and/or normal stresses). A general and consistent procedure was used for all the model simulations. We use wall functions to impose local equilibrium boundary conditions at the ground, and specify either a shear stress (for a constant stress layer host flow) or a pressure gradient aloft (for a wind tunnel or water channel boundary-layer host flow) as appropriate. Our boundary conditions are otherwise neutral in the sense that they do not mould the profiles of U, τ, and k. We adopt the observed equilibrium ratios $c_u = \sigma_u/u_{*0}$, $c_v = \sigma_v/u_{*0}$, and $c_w = \sigma_w/u_{*0}$ above the canopy (and, which effectively sets the value of the physical parameter c_e). In any event, these quantities do not vary greatly from canopy to canopy, or from one equilibrium layer to another and, as such, one common set of values could have been adopted for these quantities with no appreciable differences in the final results. We use measured C_dA to ensure that in the canopy, whatever the wind speed, the true rate of momentum extraction ensues. From these inputs and with the closure constants in either the basic or alternative windflow models fixed, we obtained quite acceptable predictions of profiles of mean wind, shear stress, and TKE for almost the entire range of canopies investigated. It was found that the alternative windflow model provided the best overall conformance for a fairly wide range of canopies. The basic windflow model has the tendency to underpredict the TKE within the canopy, although this underprediction does not appear to affect its reasonably good predictions of U and τ. However, both the basic and alternative windflow models were found to underpredict severely the magnitude of the mean wind shear at the canopy top for "urban" canopies at the highest frontal area density [0.44] investigated. Hence, it is suggested that the alternative windflow model can be used probably unmodified (viz., without resorting to tuning of any model constants) for the simulation of a wide range of canopy flows, provided the frontal area densities of the "urban" canopies are not so large as to provoke skimming flow. The equilibrium partitioning of TKE for the estimation of the individual turbulent velocity variances (normal stresses) appears to provide reasonably good estimates for these quantities.

How critically have we compared model results with data? To address this question, the following points are pertinent: (1) we chose maximal simplicity in the flow modeling to minimize the introduction of flexible parameters (closure constants); (2) we insisted on using a constant bulk drag coefficient C_d within the canopy that was diagnosed (and, not

adjusted to optimize the model fit to data) from the within-canopy mean wind and shear stress profiles, with the implicit assumption that detailed information on a height-dependent C_d would usually be unavailable; (3) free parameters (e.g., c_e, c_u, d, etc.) required for the model were determined from the physical properties of the flow, and we explicitly acknowledged the role of these constants in adjusting model curves towards the data; (4) we used a single normalizing velocity scale (u_{*0}), so as to avoid imparting any misleading appearance of quality of the simulations; and, (5) we displayed modeled and observed flow quantities so as to clearly display differences. In summary, although the success of the simulations is not automatic, and depends on the experience of the user to apply the model appropriately, making necessary judgements especially where important data are uncertain, it remains that given a set of inputs, the models used here are completely objective and reproducible.

Undoubtedly, the most important user input parameter to the windflow model is the bulk drag coefficient C_d. For all practical purposes, the most important distinction between the simulations of the various canopies lies in the inclusion of the correct C_d. How to determine an appropriate *a priori* value of C_d for a given arbitrary canopy to use as a data input to the model is an outstanding problem that needs to be resolved. Unfortunately, given our current undertanding of canopy flows, it is not possible to predict the drag on the canopy from knowledge of the obstacle geometry and the behavior of the obstacles in isolation. This represents a major weakness in the practical application of the canopy windflow models proposed here. Aside from the specification of the data input C_d, perhaps the most uncertain aspects of the implied set of equations defining the windflow model is the treatment of TKE sources and sinks in the canopy. The basic and alternative windflow models used in the present paper represent but two different methods for the treatment of the TKE sources (wake production) and sinks (form drag dissipation). Our practice of writing $\epsilon = \max(\epsilon_{\rm cc}, \epsilon_{\rm fd})$ is inelegant, and possibly not even advantageous. Certainly, there is a fundamental uncertainty about how best to treat these dissipation mechanisms. How best to partition (i.e., spectrally divide) the available TKE (from the various sources such as shear production, wake production, turbulent transport) into free-air dissipation and the extra canopy dissipation arising from its interaction with the obstacles comprising the canopy remains to be resolved.

In summary, the turbulence closures used in the windflow models here, which is perhaps something like the minimum level of closure required to calculate flows reasonably well within a wide range of canopies, captures quite well features of the mean wind and turbulence in a canopy. This is encouraging because without any alteration of the closure constants for the alternative windflow model (and which have not actually been calibrated

against any particular experimental data set for canopy flows), we have achieved reasonably good simulations of laboratory and field measurements. This is perhaps surprising, for the closure makes little more than a token recognition of the complexity of canopy flows. Indeed, its sole concession to recent thought on the mechanisms of canopy flow is to invoke the plane mixing layer analogy to provide a canopy length scale. This seeming moderate success in accounting for canopy flows using rather simple models proposed here may result from the fact that the striking spatial variations of mean flow properties in a canopy can largely be explained by mean advection and turbulent diffusion (parameterized here using a gradient diffusion hypothesis) in the presence of average sources (rates of momentum extraction, kinetic energy transformations, etc.).

This page intentionally left blank

References

1. Cionco, R. M. (1965). A Mathematical Model for Air Flow in a Vegetative Canopy. *J. Appl. Meteorol.*, 4, 517–522.

2. Cowan, I. R. (1968). Mass, Heat, and Momentum Exchange between Stands of Plants and their Atmospheric Environment. *Quart. J. Roy. Meteorol. Soc.*, 94, 318–332.

3. Svensson, U. and Haggkvist, K. (1990). A Two-Equation Turbulence Model for Canopy Flows. *J. Wind Eng. Indust. Aero.*, 35, 201–211.

4. Liu, J., Chen, J. M., Black, T. A., and Novak, M. D. (1996). E-ϵ Modeling of Turbulent Air Flow Downwind of a Model Forest Edge. *Boundary-Layer Meteorol.*, 77, 21–44.

5. Wilson, N. R. and Shaw, R. H. (1977). A Higher-Order Closure Model for Canopy Flow. *J. Appl. Meteorol.*, 16, 1197–1205.

6. Wilson, J. D. (1988). A Second-Order Closure Model for Flow Through Vegetation. *Boundary-Layer Meteorol.*, 42, 371–392.

7. Massman, W. J. (1997). An Analytical One-Dimensional Model of Momentum Transfer by Vegetation of Arbitrary Structure. *Boundary-Layer Meteorol.*, 83, 407–421.

8. Meyers, T. and Paw U, K. T. (1986). Testing of a Higher-Order Closure Model for Modeling Airflow Within and Above Plant Canopies. *Boundary-Layer Meteorol.*, 37, 297–311.

9. Raupach, M. R. (1988). Canopy Transport Processes. In W. L. Steffen and O. T. Denmead (eds), *Flow and Transport in the Natural Environment*, Springer-Verlag, New York.

10. Yee, E. and Wilson, J. D. (2000). Model for the Mean Wind and Turbulence Within and Above an Urban Canopy, Part I: Theory and Numerical Implementation. DRES TR 2000-020, Defence Research Establishment Suffield, 36 pp.

11. Townsend, A. A. (1976). *The Structure of Turbulent Shear Flow*, Second Edition, Cambridge University Press, Cambridge, England.

12. Delage, Y. (1974). A Numerical Study of the Nocturnal Atmospheric Boundary-Layer. *Q. J. Roy. Meteorol. Soc.*, 100, 351–364.

13. Raupach, M. R., Finnigan, J. J., and Brunet, Y. (1996). Coherent Eddies and Turbulence in Vegetation Canopies: The Mixing-Layer Analogy. *Boundary-Layer Meteorol.*, 78, 351–382.

14. Wilson, J. D., Finnigan, J. J., and Raupach, M. R. (1998). A First-Order Closure for Disturbed Plant-Canopy Flows, and Its Application to Winds in a Canopy on a Ridge. *Q. J. Roy. Meteorol. Soc.*, 124, 705–732.

15. Brunet, Y., Finnigan, J. J., and Raupach, M. R. (1994). A Wind Tunnel Study of Air Flow in Waving Wheat: Single-Point Velocity Statistics. *Boundary-Layer Meteorol.*, 70, 95–132.

16. Launder, B. E. and Spalding, D. B. (1972). *Mathematical Methods of Turbulence*, Academic Press, London, England.

17. Launder, B. E. and Spalding, D. B. (1974). The Numerical Computation of Turbulent Flows. *Comput. Methods Appl. Mech. Eng.*, 3, 169–189.

18. Brunet, Y., Finnigan, J. J., and Raupach, M. R. (1994). A Wind Tunnel Study of Air Flow in Waving Wheat: Single-Point Velocity Statistics. *Boundary-Layer Meteorol.*, 70, 95–132.

19. Finnigan, J. J. and Brunet, Y. (1995). Turbulent Airflow in Forests on Flat and Hilly Terrain. In M. P. Coutts and J. Grace (eds), *Wind and Trees*, Cambridge University Press, UK.

20. Wilson, J. D., Ward, D. P., Thurtell, G. W., and Kidd, G. E. (1982). Statistics of Atmospheric Turbulence Within and Above a Corn Canopy. *Boundary-Layer Meteorol.*, 24, 495–519.

21. Macdonald, R. W., Carter, S., and Slawson, P. R. (2000). Measurements of Mean Velocity and Turbulence Statistics in Simple Obstacle Arrays at 1:200 Scale. Thermal Fluids Report 2000–1, University of Waterloo, 128 pp.

22. Raupach, M. R., Coppin, P. A., and Legg, B. J. (1986). Experiments on Scalar Dispersion Within a Model Plant Canopy. Part I: The Turbulence Structure. *Boundary-Layer Meteorol.*, 39, 21–52.

23. Legg, B. J., Coppin, P. C., and Raupach, M. R. (1984). A Three-Hot-Wire Anemometer for Measuring Two Velocity Components in High Intensity Turbulent Boundary-Layers. *J. Phys. E*, 17, 970–976.

24. Van Doormaal, J. P. and Raithby, G. D. (1984). Enhancements of the SIMPLE Method for Predicting Incompressible Fluid Flows. *Numerical Heat Transfer*, 7, 147–163.

25. Macdonald, R. W., Griffiths, R. F., and Hall, D. J. (1998). An Improved Method for the Estimation of Surface Roughness of Obstacle Arrays. *Atmos. Environ.*, 32, 1857–1864.

26. Lumley, J. L. (1978). Computational Modeling of Turbulent Flows. *Adv. Appl. Mech.*, 18, 123–176.

27. Rogers, M. M. and Moser, R. D. (1994). Direct Simulation of a Self-Similar Turbulent Mixing Layer. *Phys. Fluids*, 6, 903–922.

This page intentionally left blank

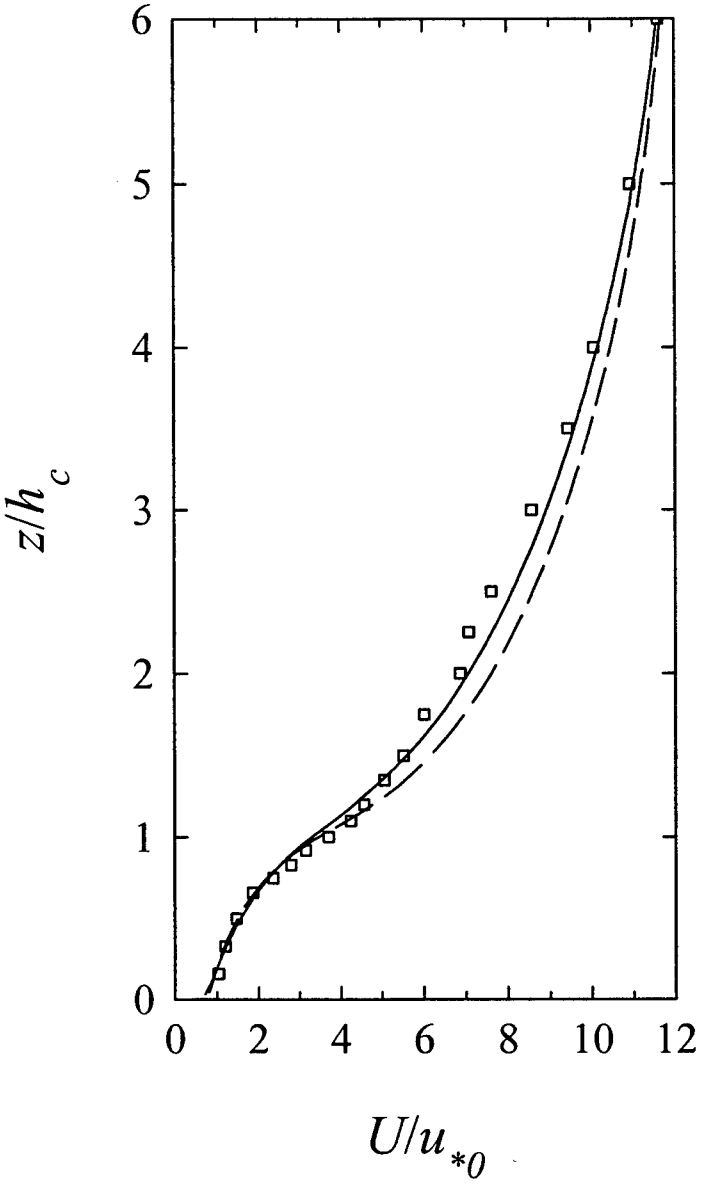

Figure 1. *Mean wind speed observed in and above a model aeroelastic plant canopy in a wind-tunnel boundary-layer (Furry Hill experiment) compared with the outcome of model simulations using the basic (solid curve) and alternative (long dashed curve) canopy windflow models.*

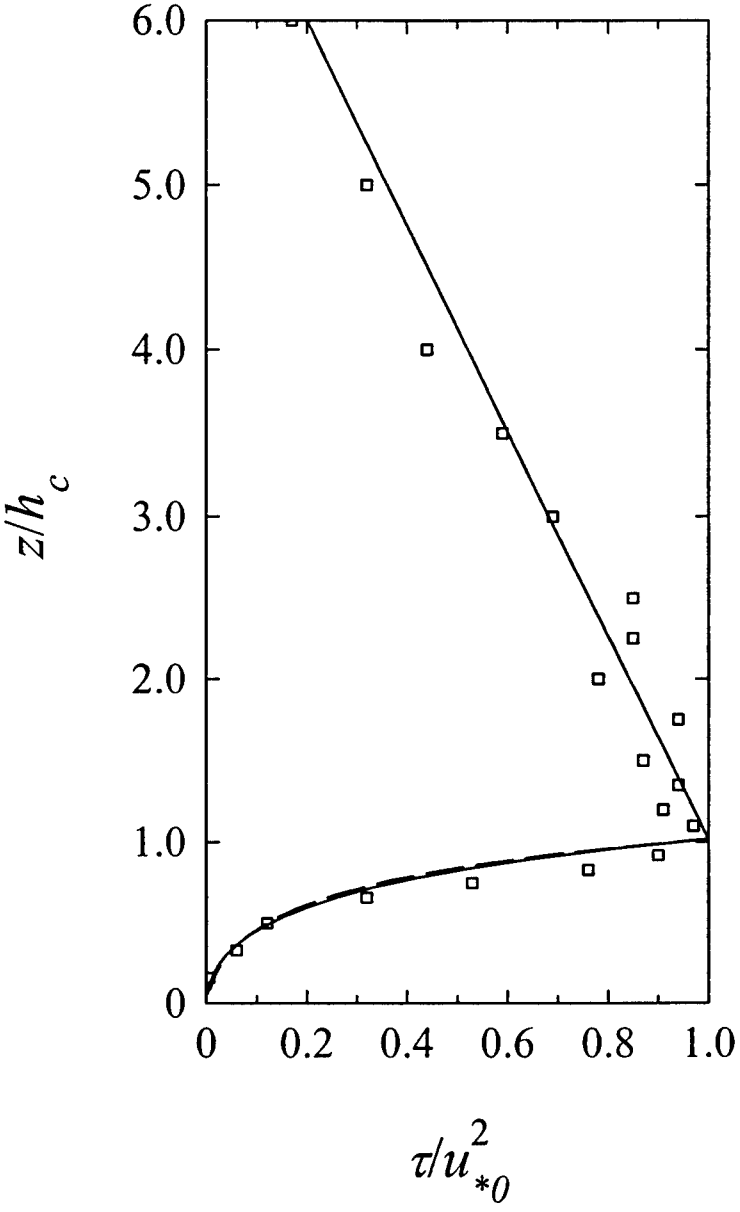

Figure 2. *Shear stress observed in and above a model aeroelastic plant canopy in a wind-tunnel boundary-layer (Furry Hill experiment) compared with the outcome of model simulations using the basic (solid curve) and alternative (long dashed curve) canopy windflow models.*

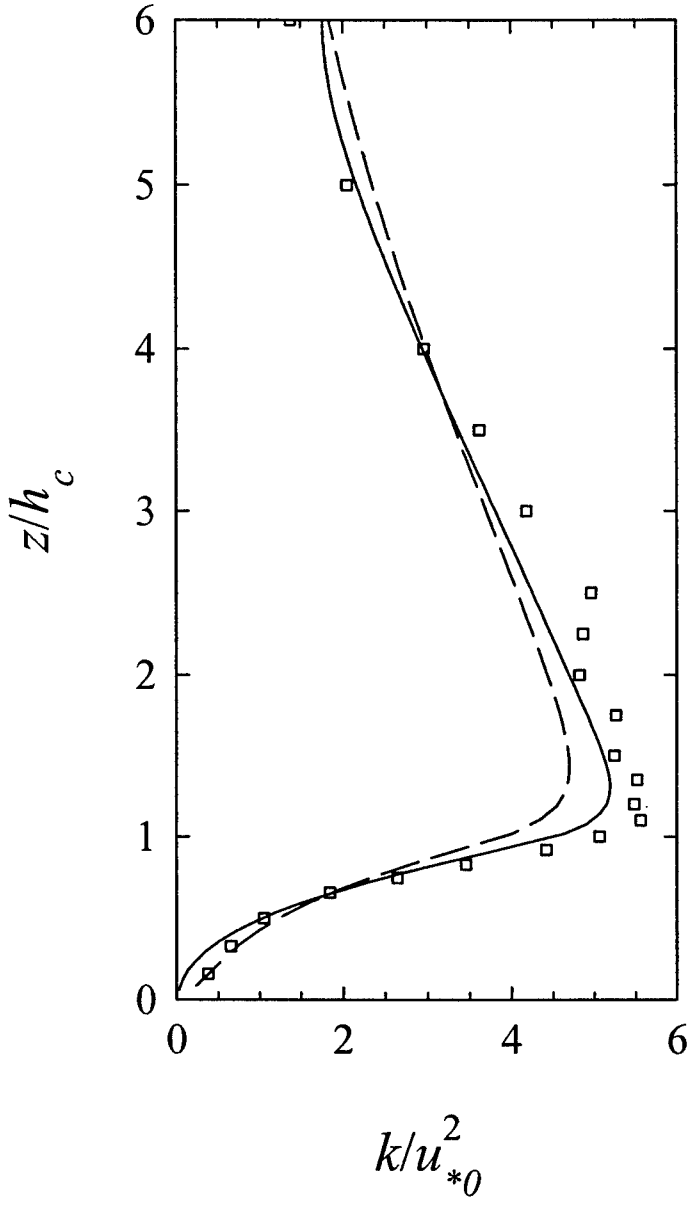

Figure 3. *Turbulence kinetic energy observed in and above a model aeroelastic plant canopy in a wind-tunnel boundary-layer (Furry Hill experiment) compared with the outcome of model simulations using the basic (solid curve) and alternative (long dashed curve) canopy windflow models.*

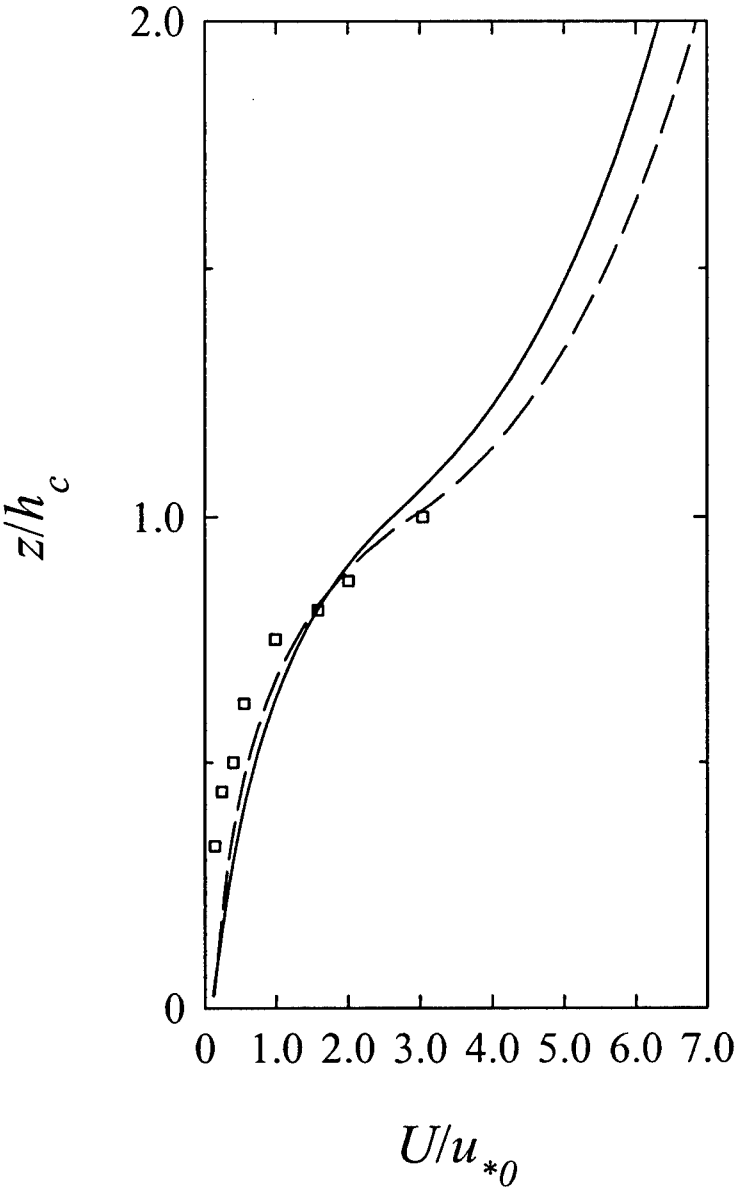

Figure 4. *Mean wind speed observed in a canopy of corn (Elora, Ontario) compared with the outcome of model simulations using the basic (solid curve) and alternative (long dashed curve) canopy windflow models.*

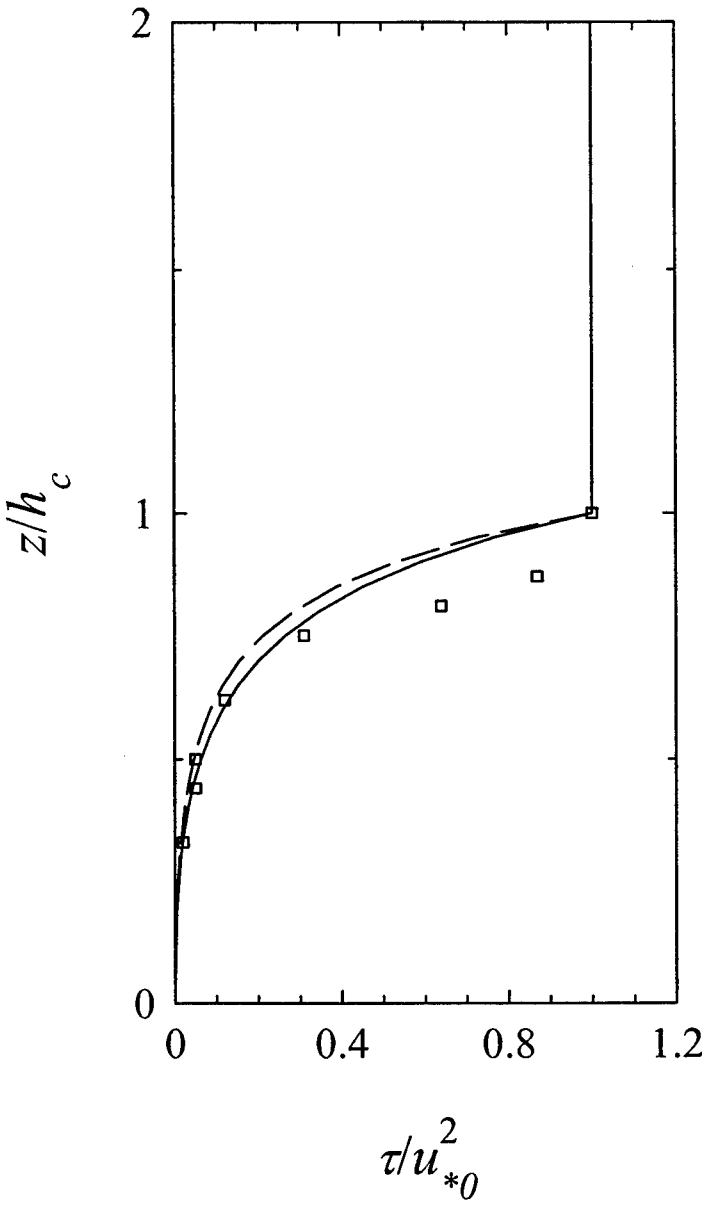

Figure 5. *Shear stress observed in a canopy of corn (Elora, Ontario) compared with the outcome of model simulations using the basic (solid curve) and alternative (long dashed curve) canopy windflow models.*

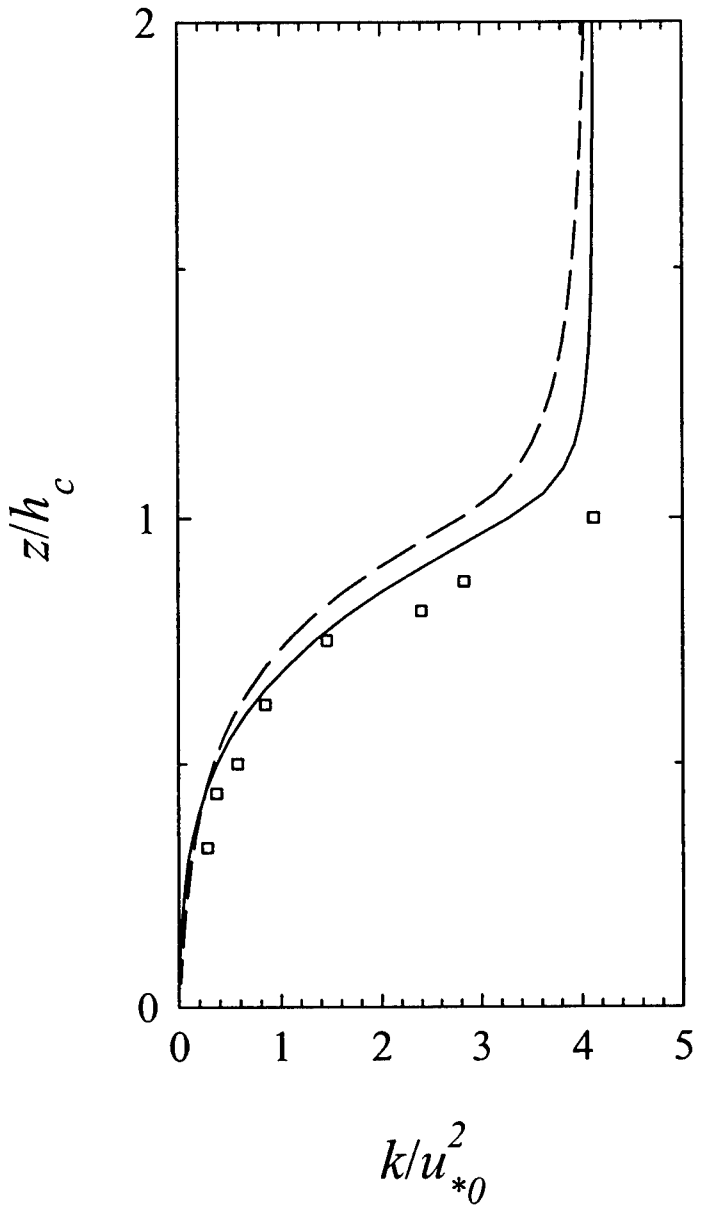

Figure 6. *Turbulence kinetic energy observed in a canopy of corn (Elora, Ontario) compared with the outcome of model simulations using the basic (solid curve) and alternative (long dashed curve) canopy windflow models.*

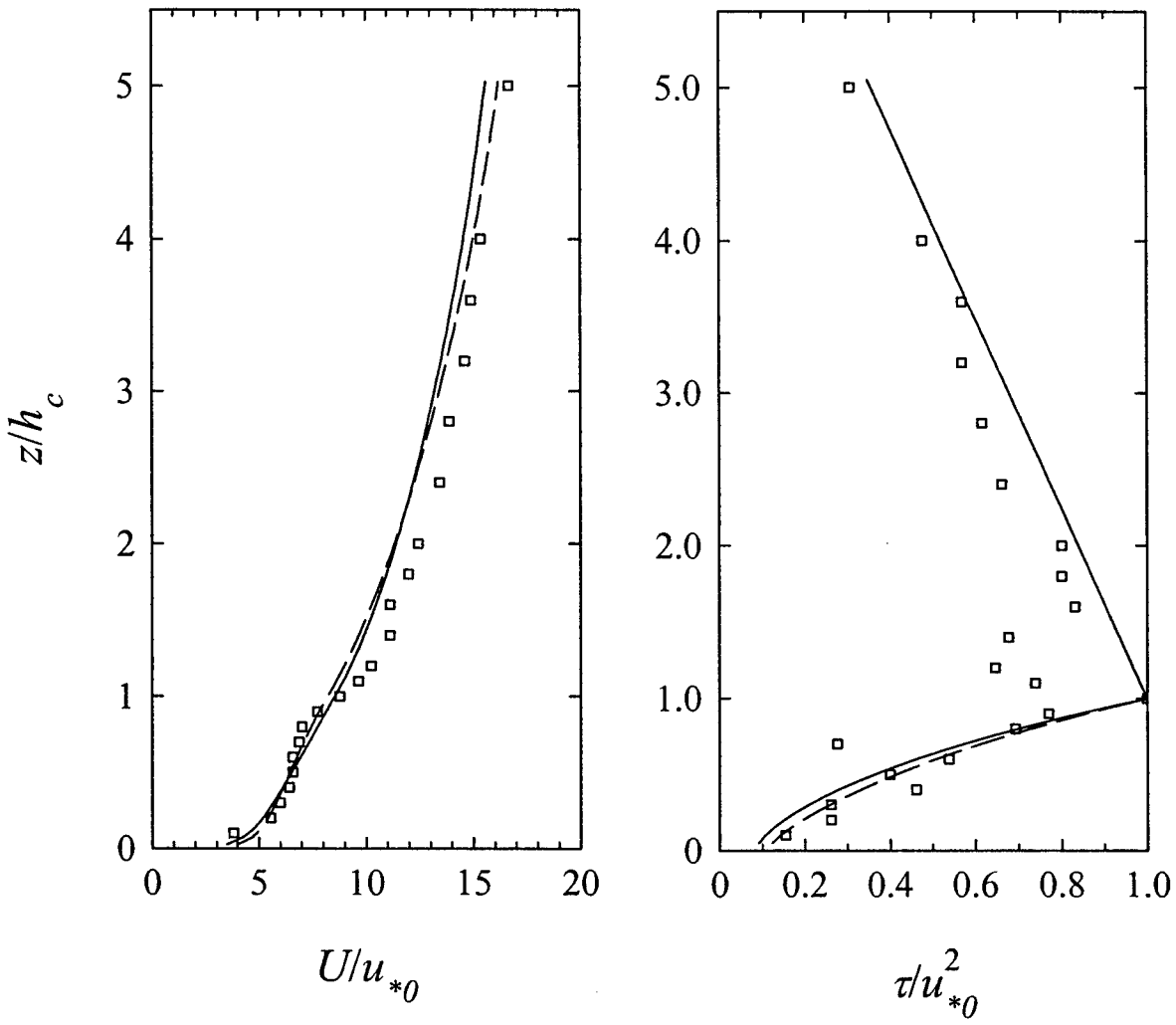

Figure 7. *Mean wind speed (left panel) and shear stress (right panel) observed in and above a square array of cubical obstacles with a frontal area index of 0.0625 compared with the outcome of model simulations using the basic (solid curve) and alternative (long dashed curve) canopy windflow models.*

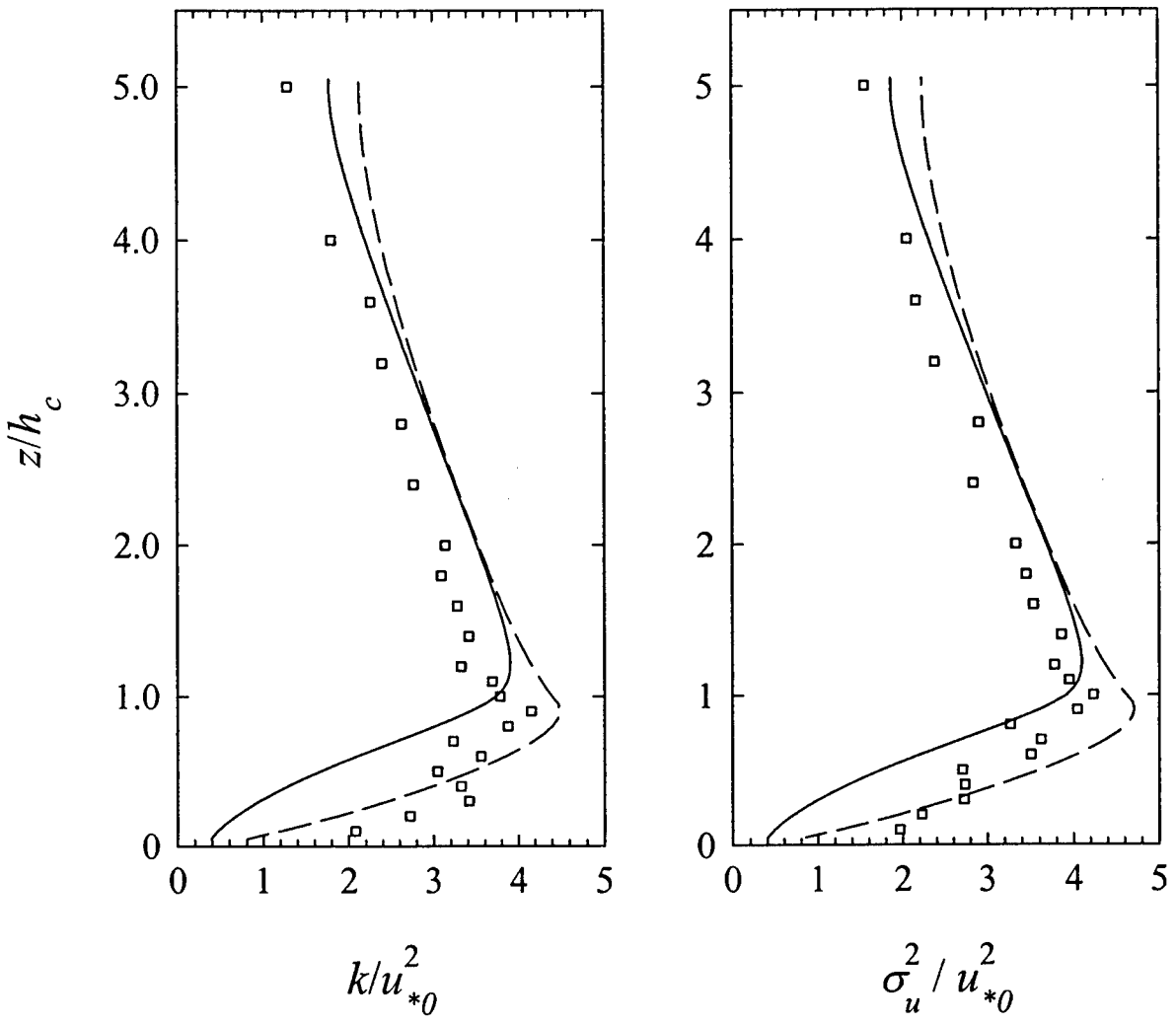

Figure 8. *Turbulence kinetic energy (left panel) and streamwise velocity variance (right panel) observed in and above a square array of cubical obstacles with a frontal area index of 0.0625 compared with the outcome of model simulations using the basic (solid curve) and alternative (long dashed curve) canopy windflow models.*

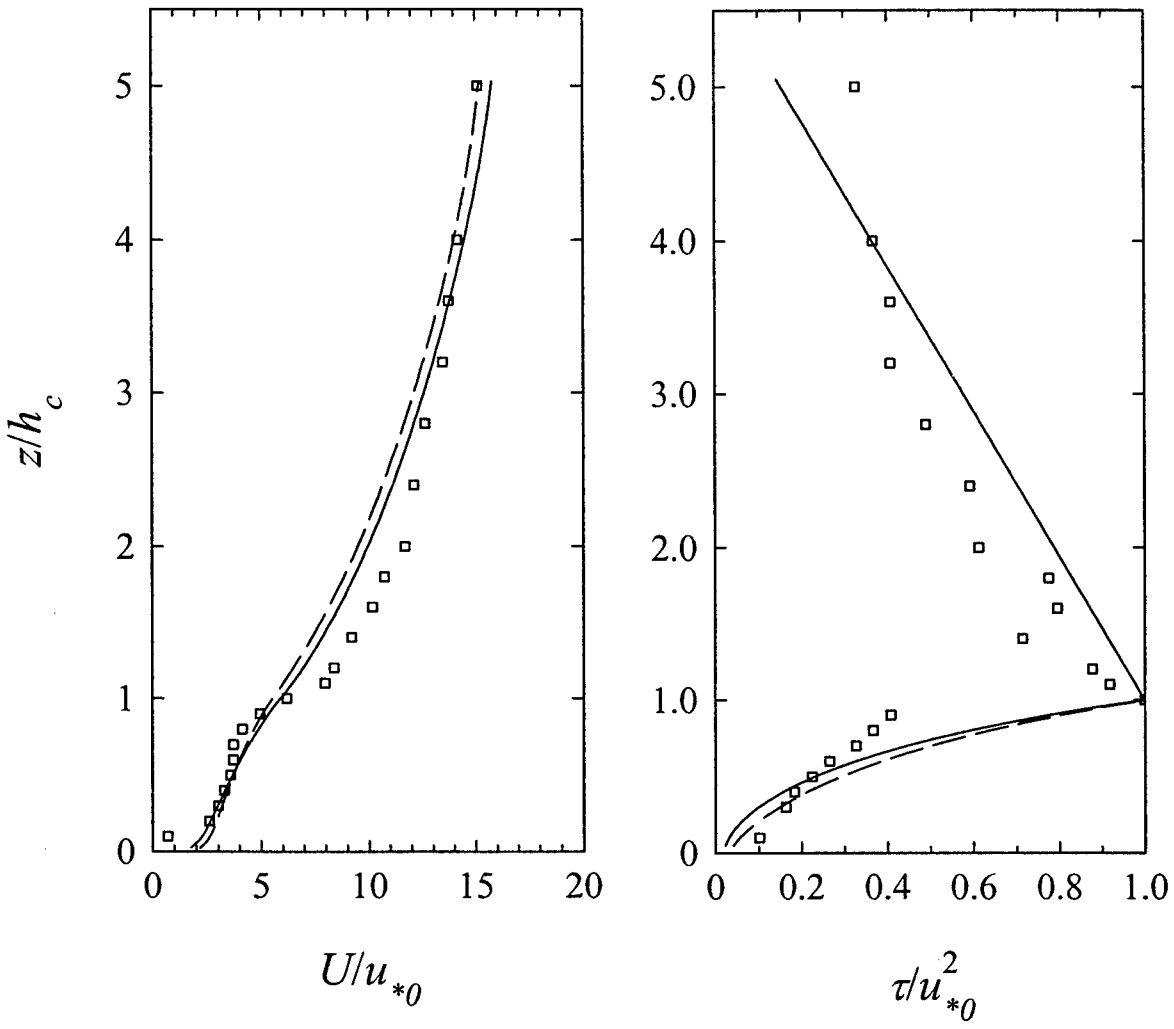

Figure 9. *Mean wind speed (left panel) and shear stress (right panel) observed in and above a square array of cubical obstacles with a frontal area index of 0.16 compared with the outcome of model simulations using the basic (solid curve) and alternative (long dashed curve) canopy windflow models.*

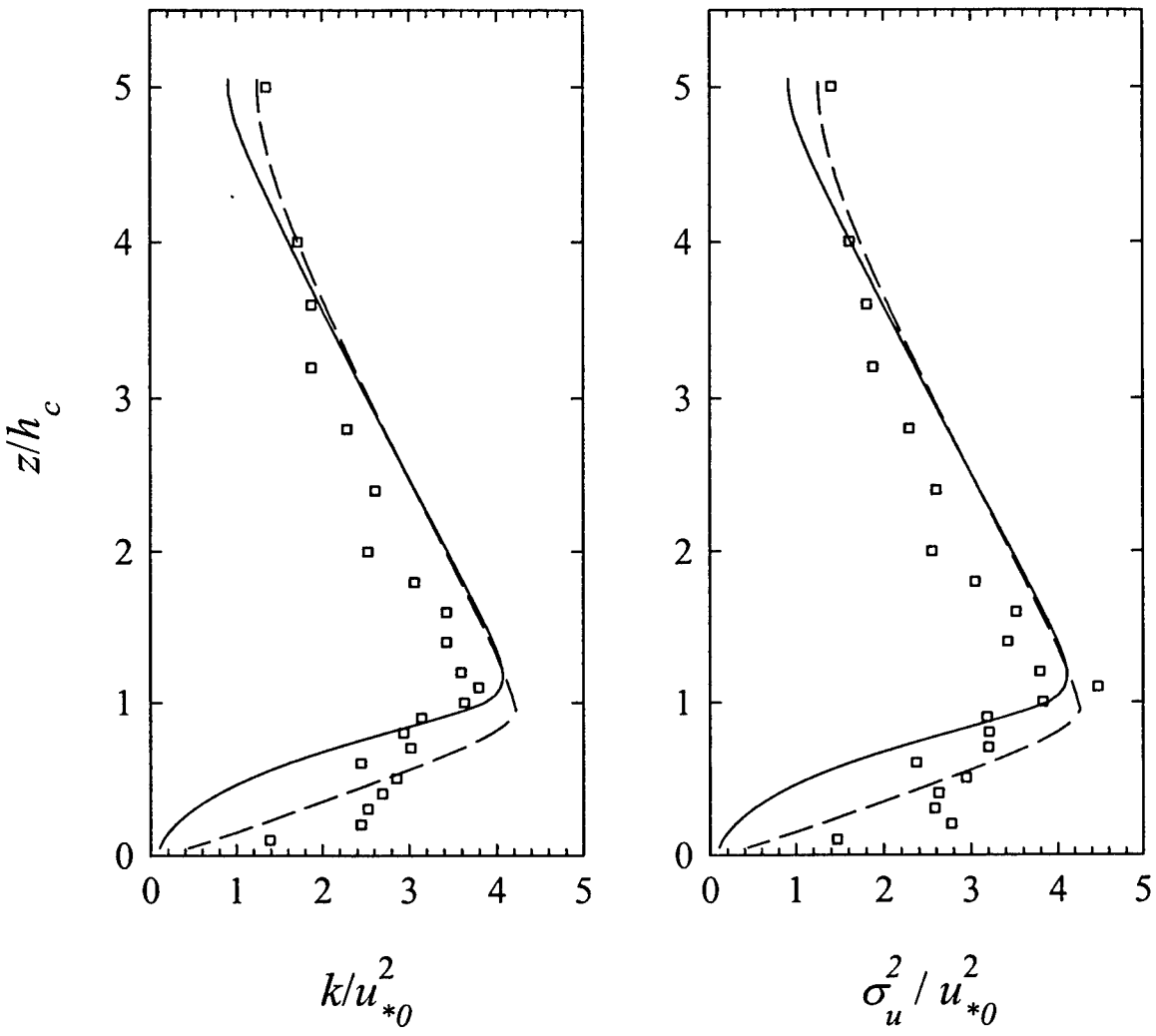

Figure 10. *Turbulence kinetic energy (left panel) and streamwise velocity variance (right panel) observed in and above a square array of cubical obstacles with a frontal area index of 0.16 compared with the outcome of model simulations using the basic (solid curve) and alternative (long dashed curve) canopy windflow models.*

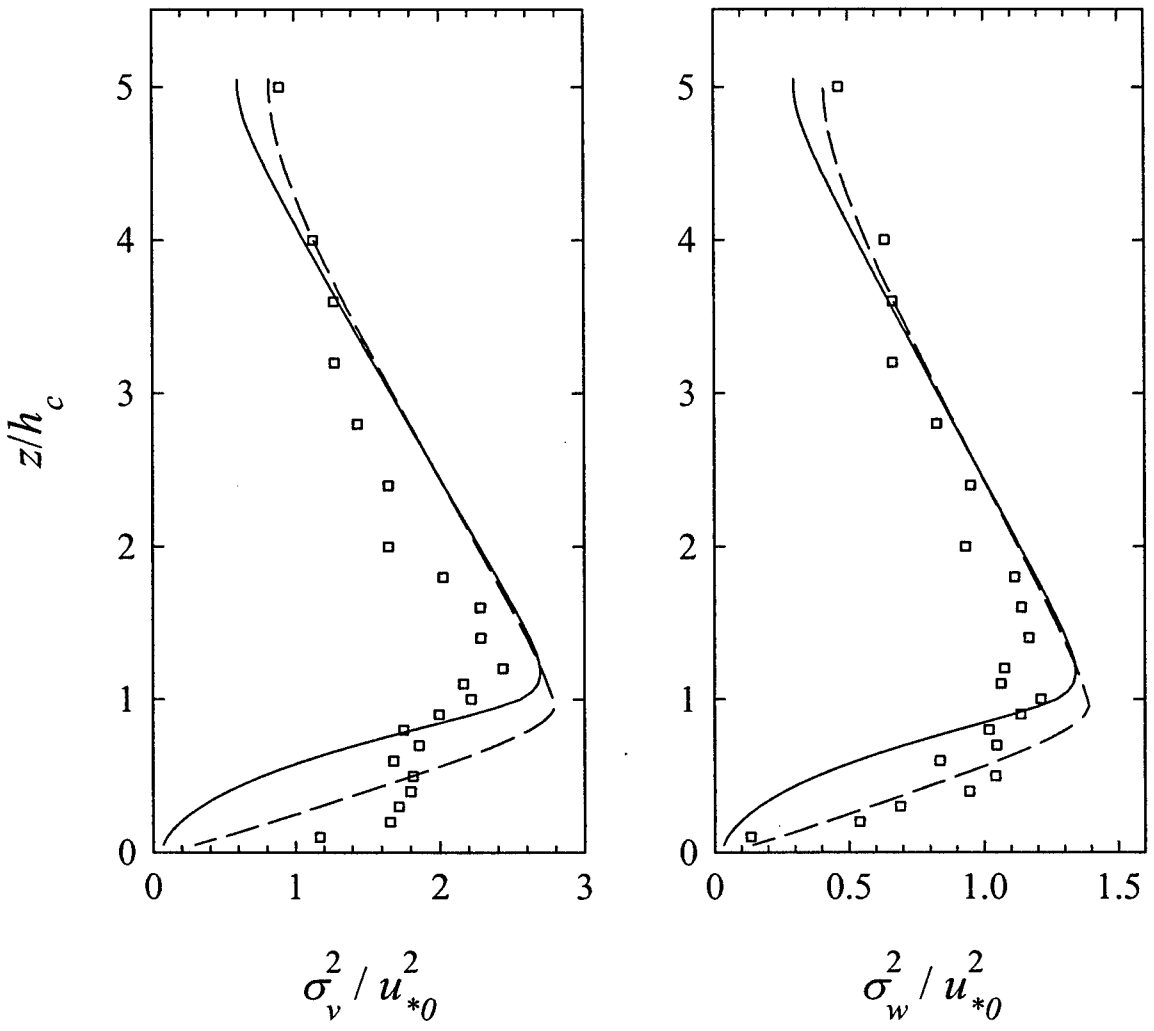

Figure 11. *Cross-stream velocity variance (left panel) and vertical velocity variance (right panel) observed in and above a square array of cubical obstacles with a frontal area index of 0.16 compared with the outcome of model simulations using the basic (solid curve) and alternative (long dashed curve) canopy windflow models.*

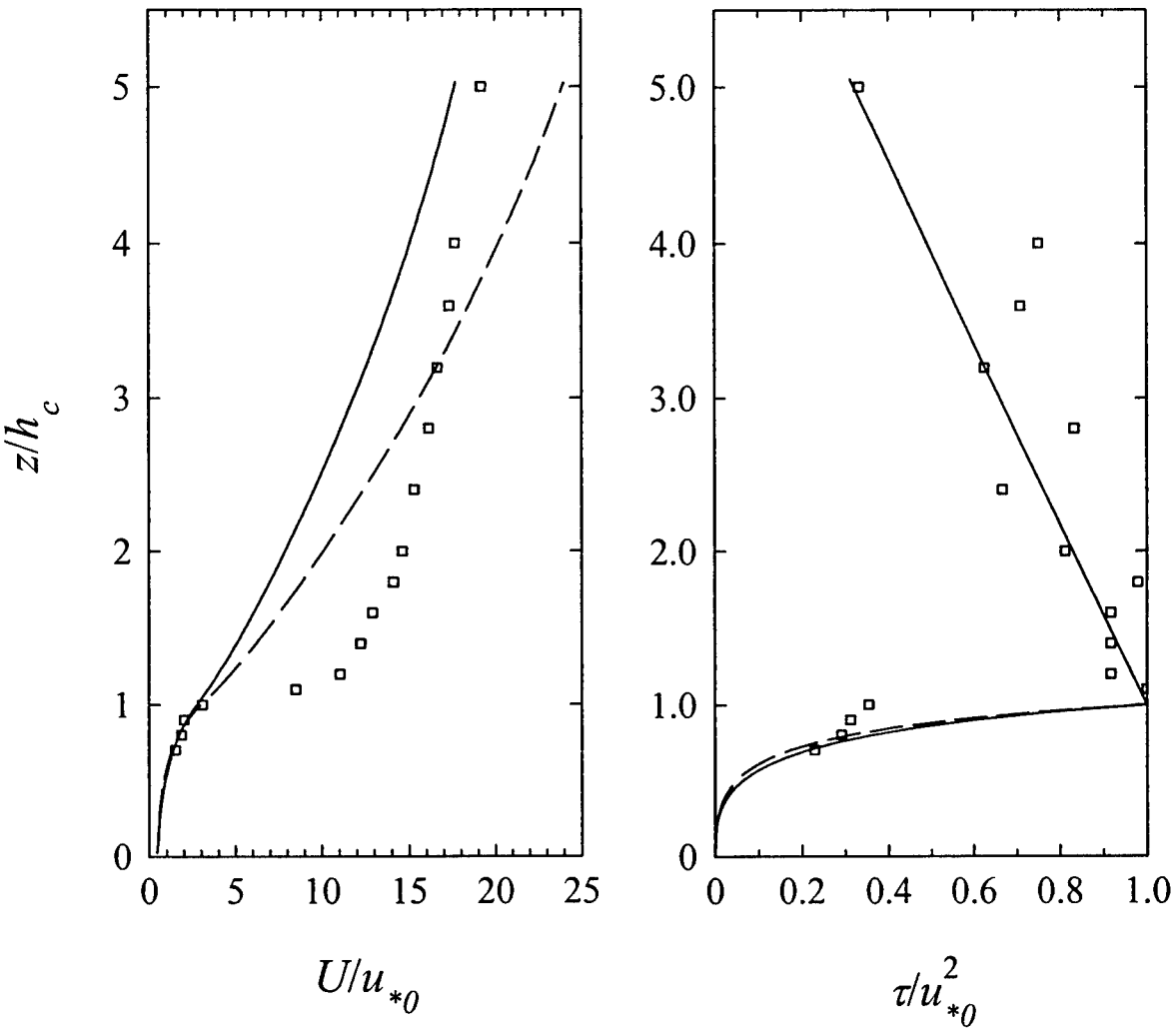

Figure 12. *Mean wind speed (left panel) and shear stress (right panel) observed in and above a square array of cubical obstacles with a frontal area index of 0.44 compared with the outcome of model simulations using the basic (solid curve) and alternative (long dashed curve) canopy windflow models.*

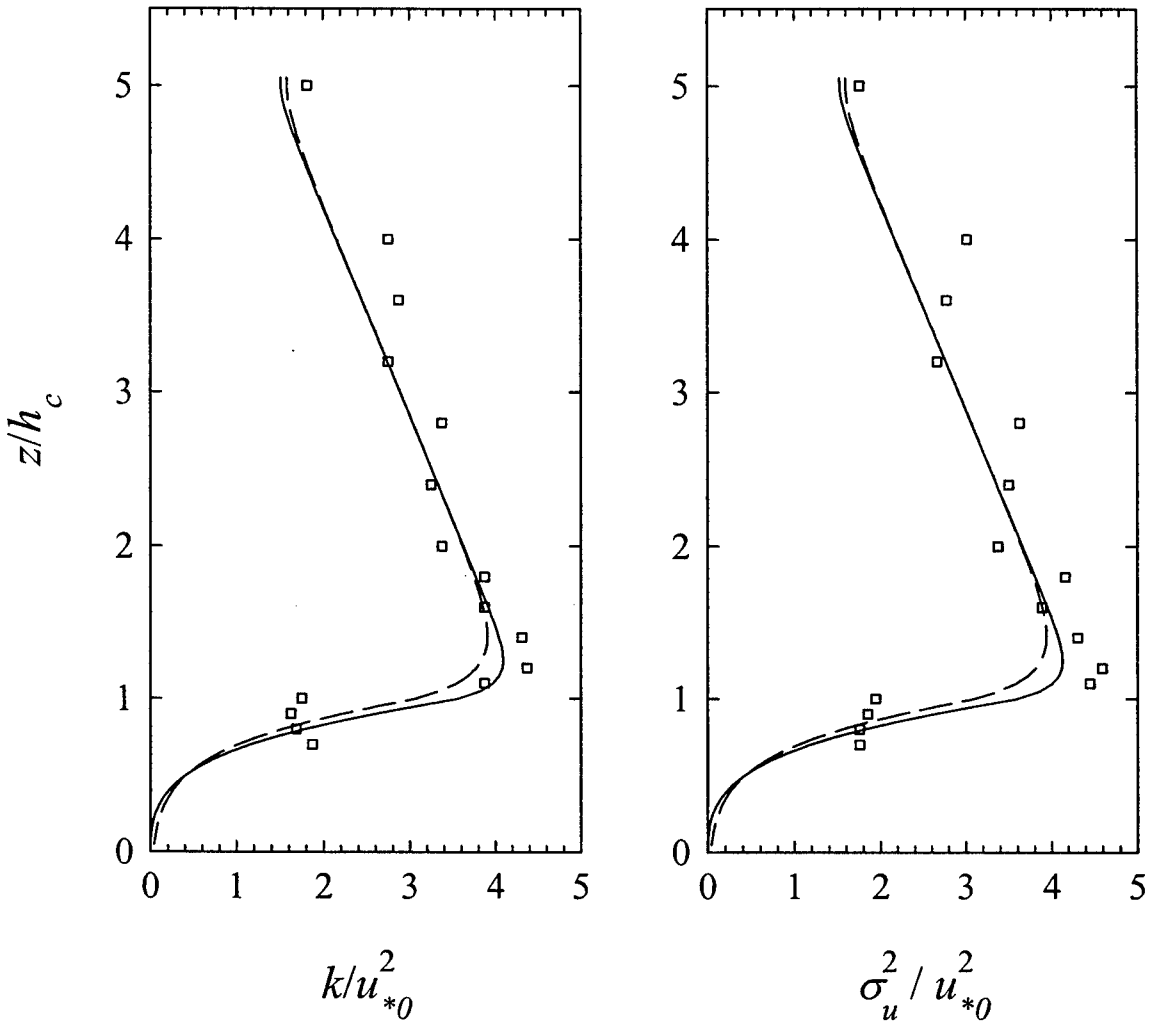

Figure 13. *Turbulence kinetic energy (left panel) and streamwise velocity variance (right panel) observed in and above a square array of cubical obstacles with a frontal area index of 0.44 compared with the outcome of model simulations using the basic (solid curve) and alternative (long dashed curve) canopy windflow models.*

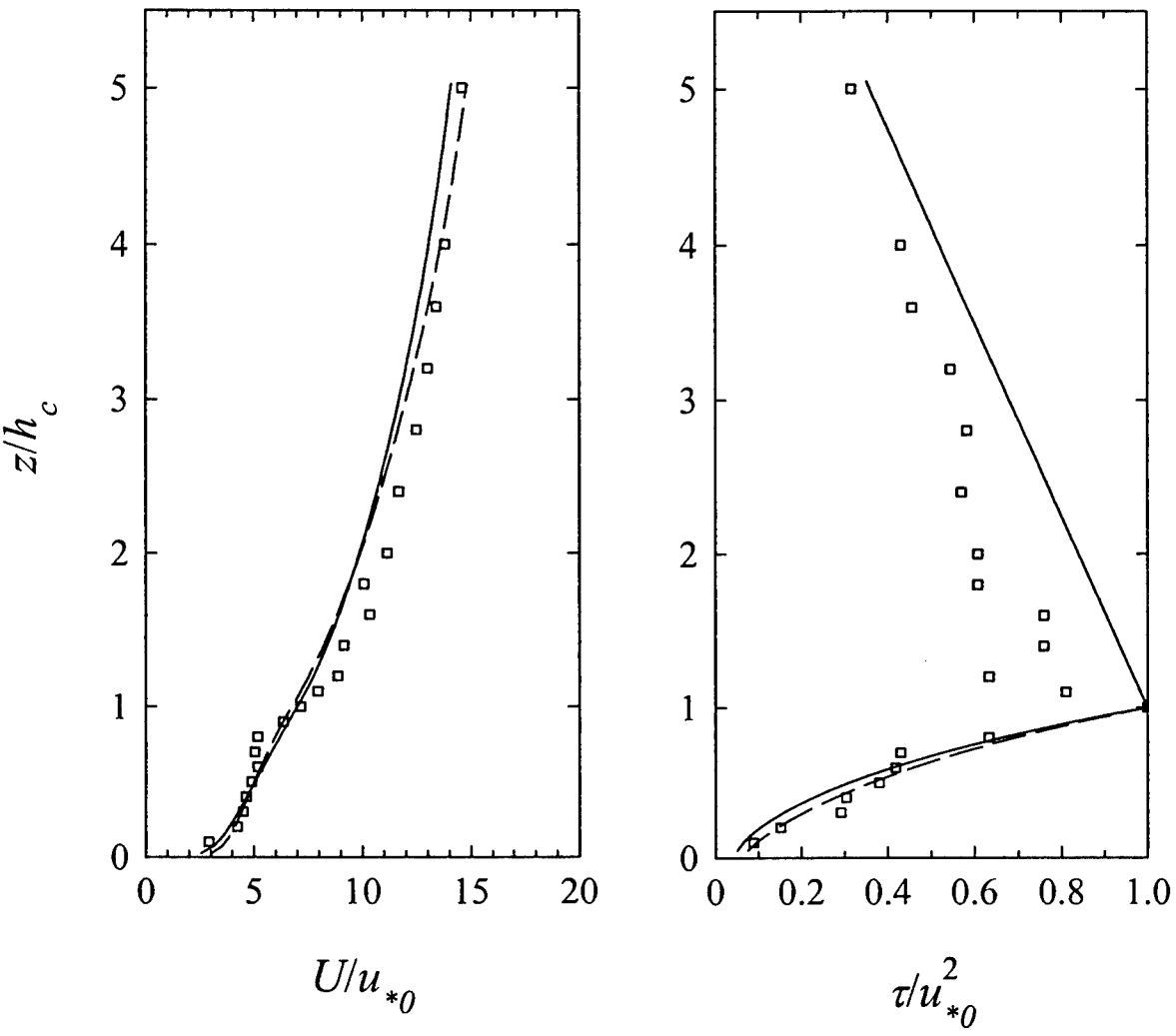

Figure 14. *Mean wind speed (left panel) and shear stress (right panel) observed in and above a staggered array of cubical obstacles with a frontal area index of 0.0625 compared with the outcome of model simulations using the basic (solid curve) and alternative (long dashed curve) canopy windflow models.*

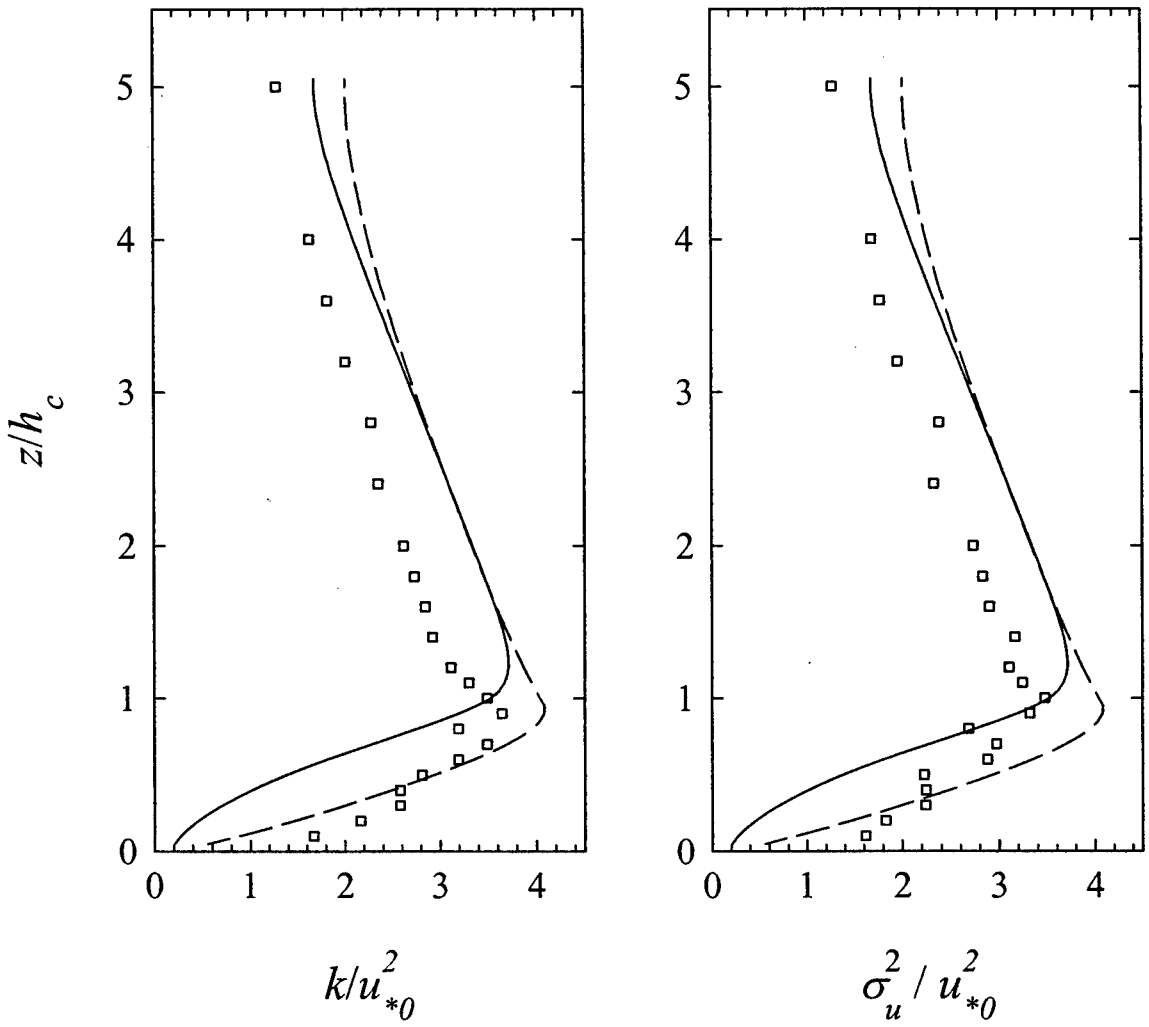

Figure 15. *Turbulence kinetic energy (left panel) and streamwise velocity variance (right panel) observed in and above a staggered array of cubical obstacles with a frontal area index of 0.0625 compared with the outcome of model simulations using the basic (solid curve) and alternative (long dashed curve) canopy windflow models.*

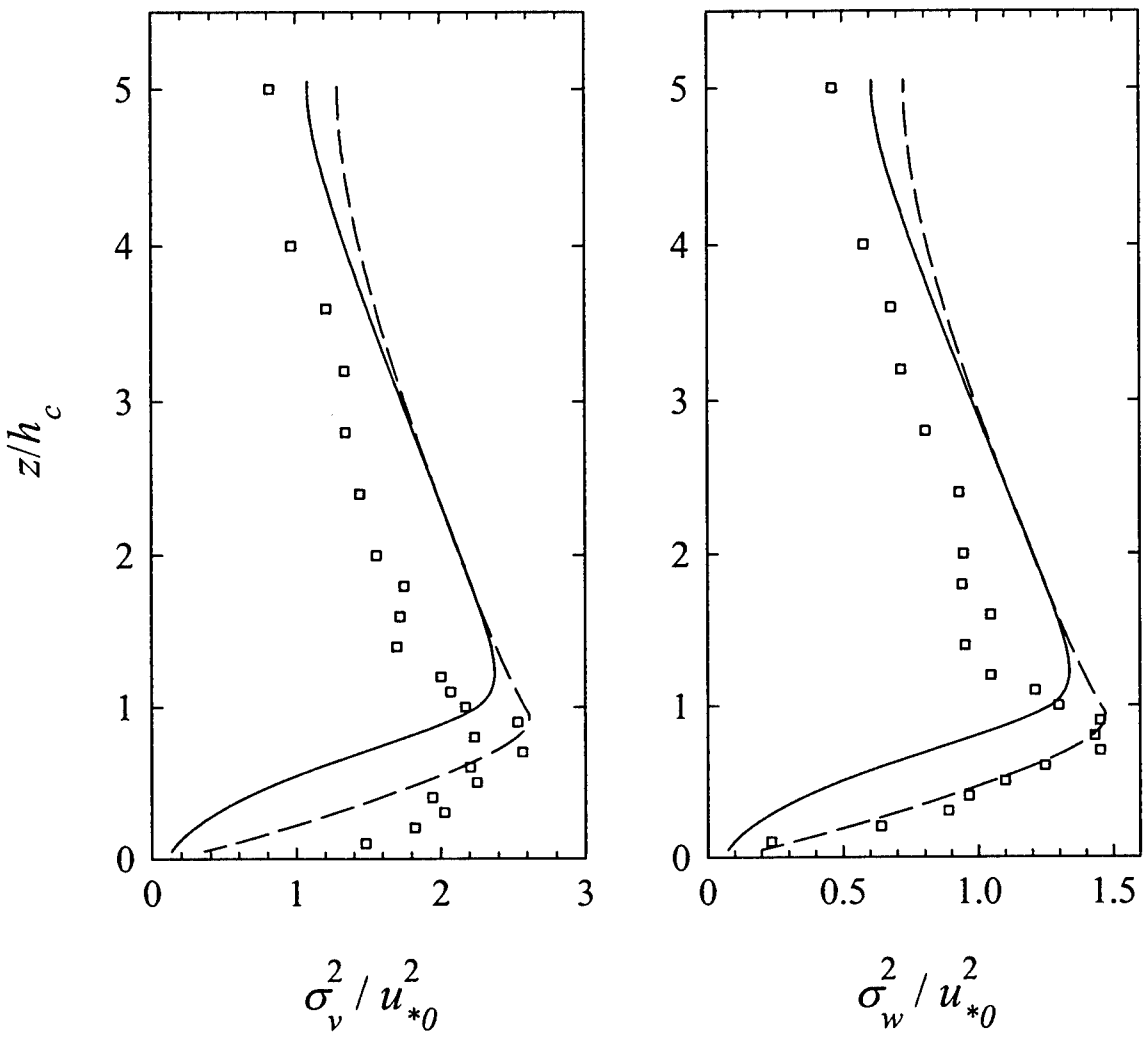

Figure 16. *Cross-stream velocity variance (left panel) and vertical velocity variance (right panel) observed in and above a staggered array of cubical obstacles with a frontal area index of 0.0625 compared with the outcome of model simulations using the basic (solid curve) and alternative (long dashed curve) canopy windflow models.*

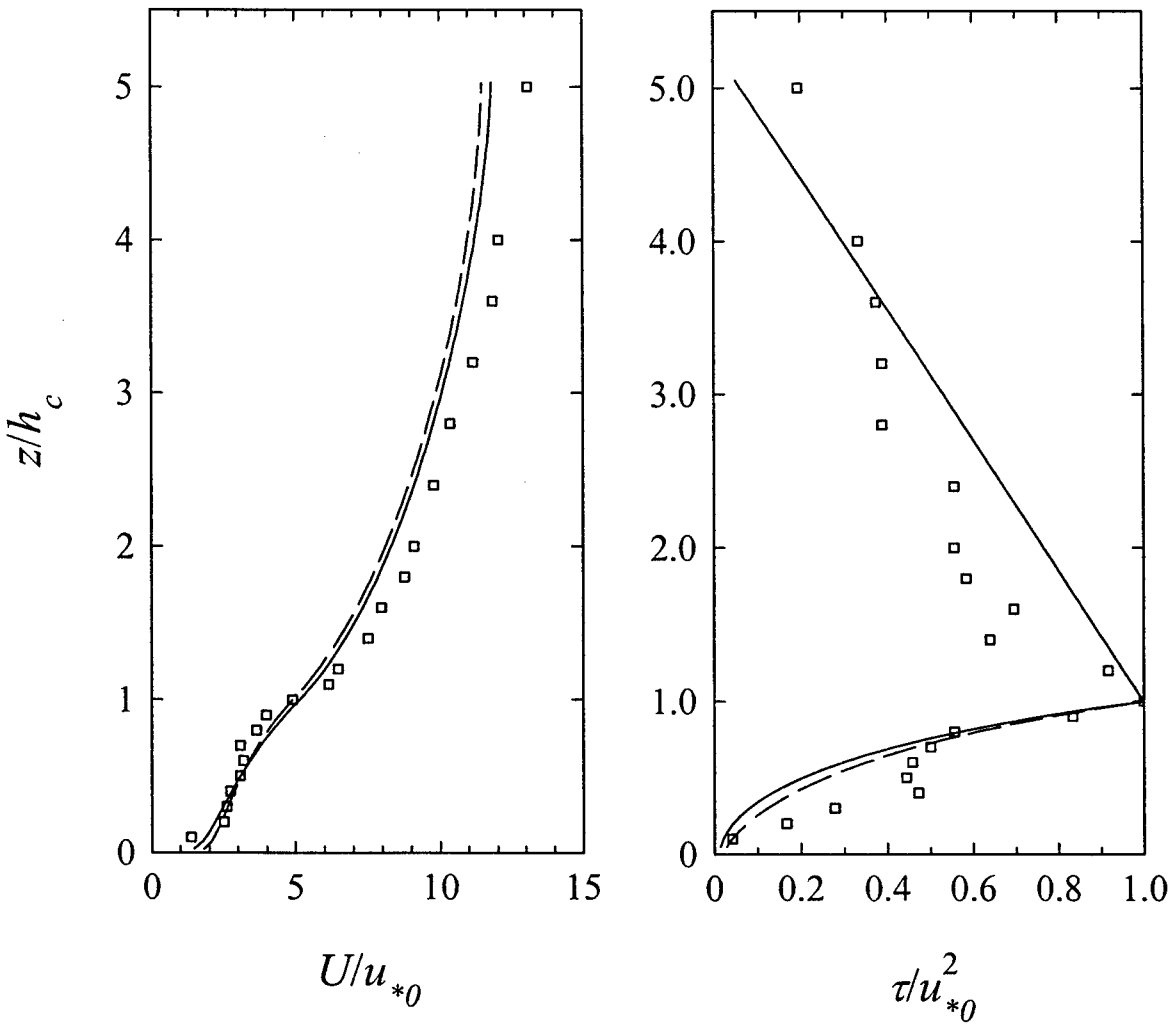

Figure 17. *Mean wind speed (left panel) and shear stress (right panel) observed in and above a staggered array of cubical obstacles with a frontal area index of 0.16 compared with the outcome of model simulations using the basic (solid curve) and alternative (long dashed curve) canopy windflow models.*

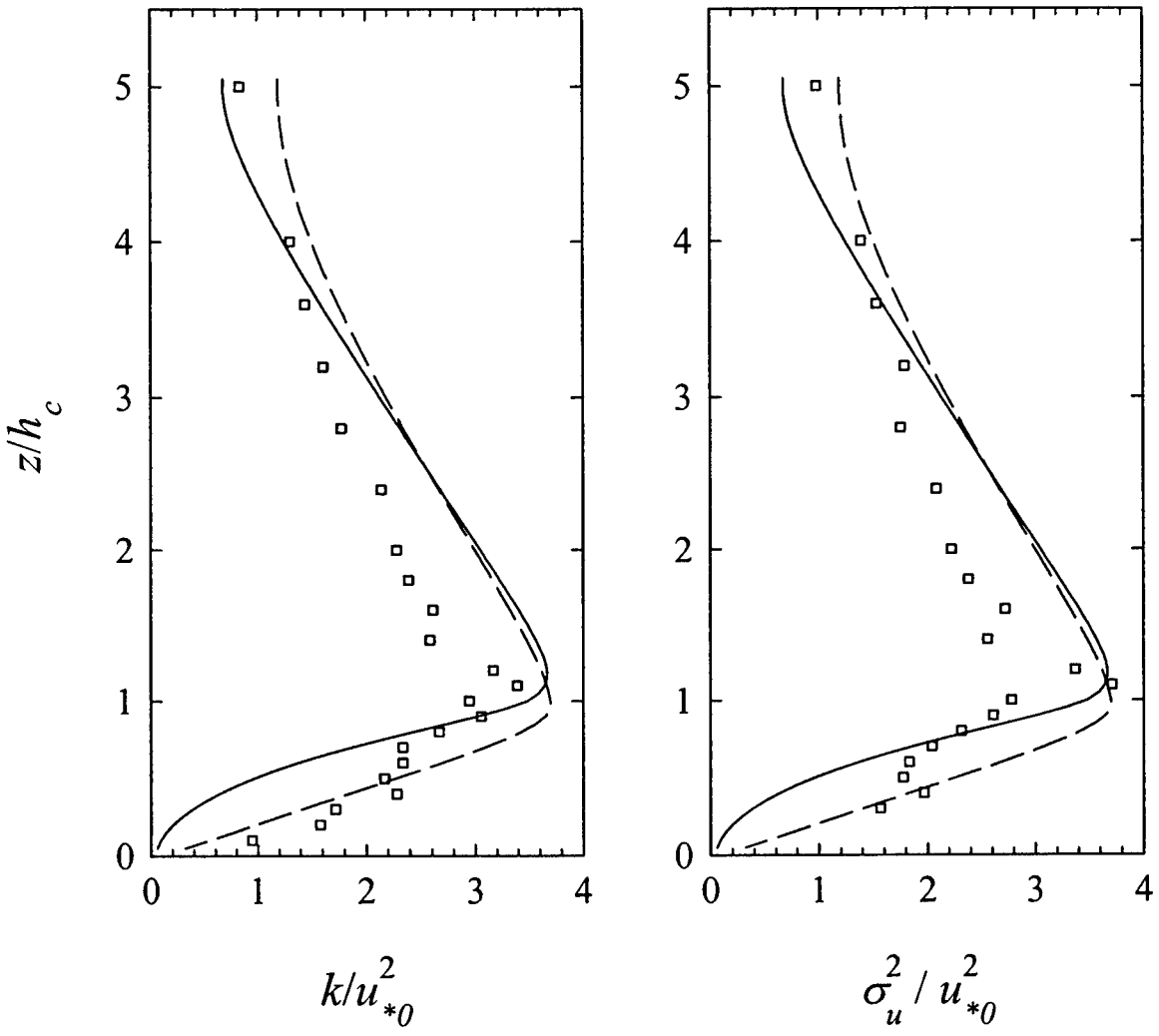

Figure 18. *Turbulence kinetic energy (left panel) and streamwise velocity variance (right panel) observed in and above a staggered array of cubical obstacles with a frontal area index of 0.16 compared with the outcome of model simulations using the basic (solid curve) and alternative (long dashed curve) canopy windflow models.*

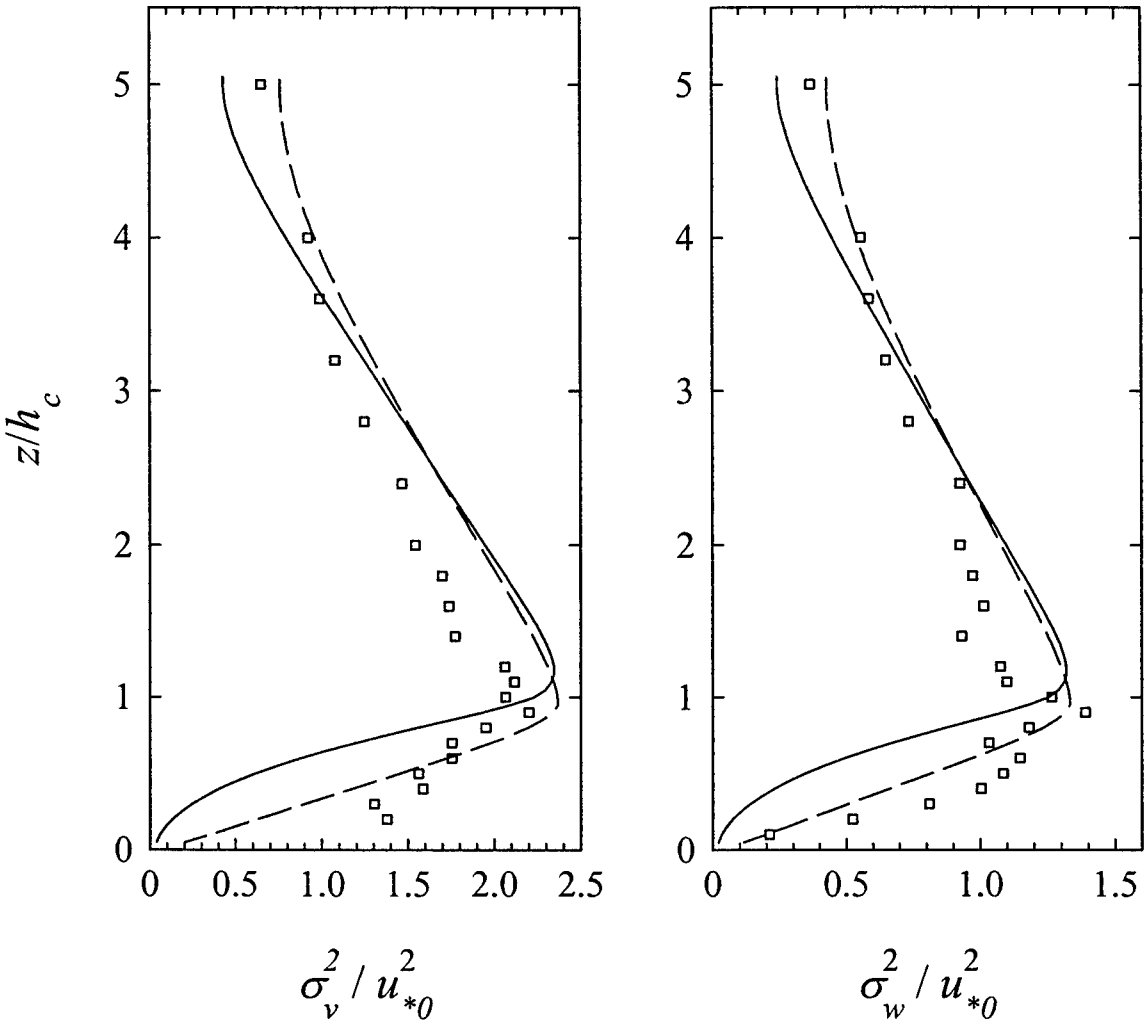

Figure 19. *Cross-stream velocity variance (left panel) and vertical velocity variance (right panel) observed in and above a staggered array of cubical obstacles with a frontal area index of 0.0625 compared with the outcome of model simulations using the basic (solid curve) and alternative (long dashed curve) canopy windflow models.*

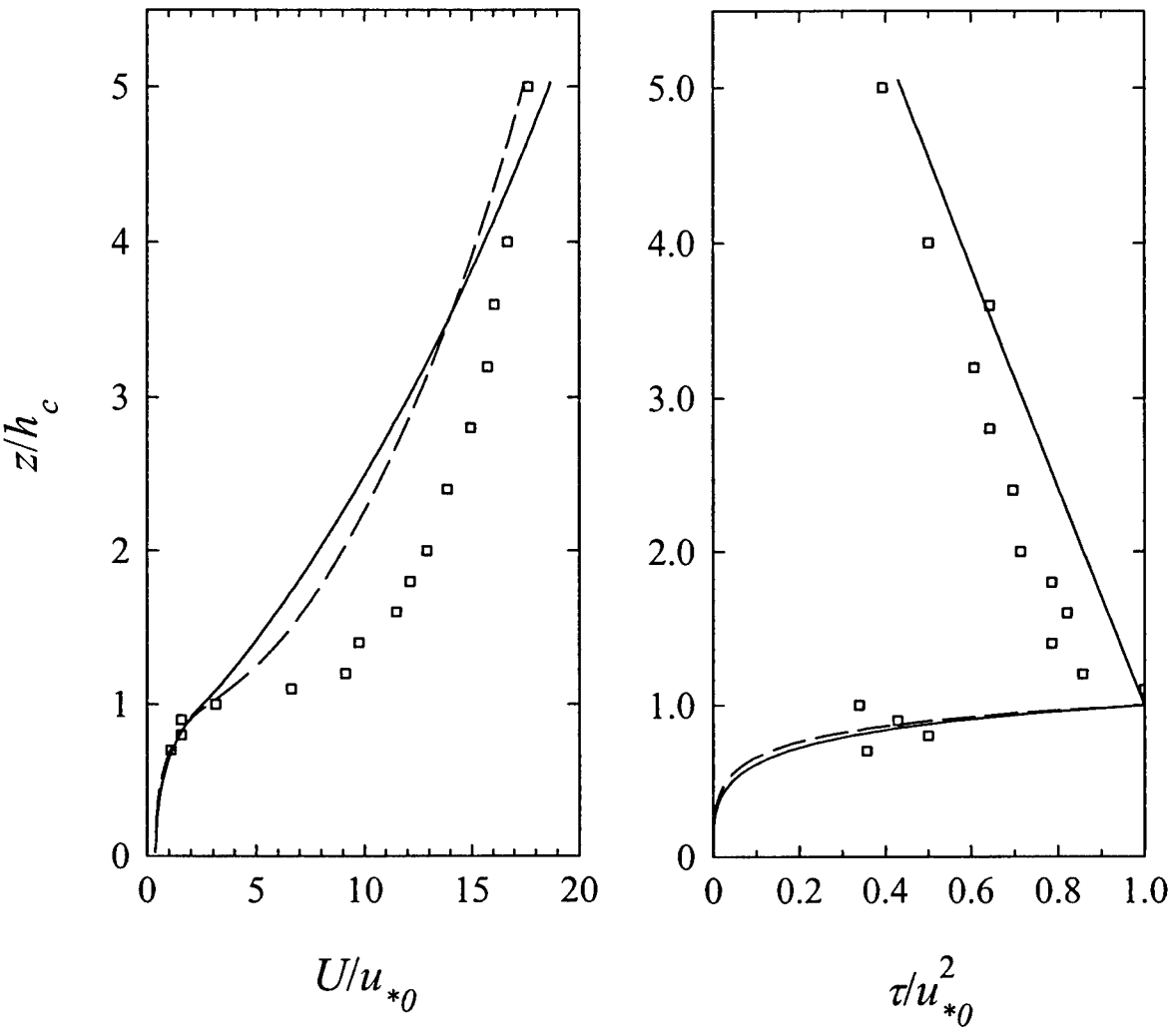

Figure 20. *Mean wind speed (left panel) and shear stress (right panel) observed in and above a staggered array of cubical obstacles with a frontal area index of 0.44 compared with the outcome of model simulations using the basic (solid curve) and alternative (long dashed curve) canopy windflow models.*

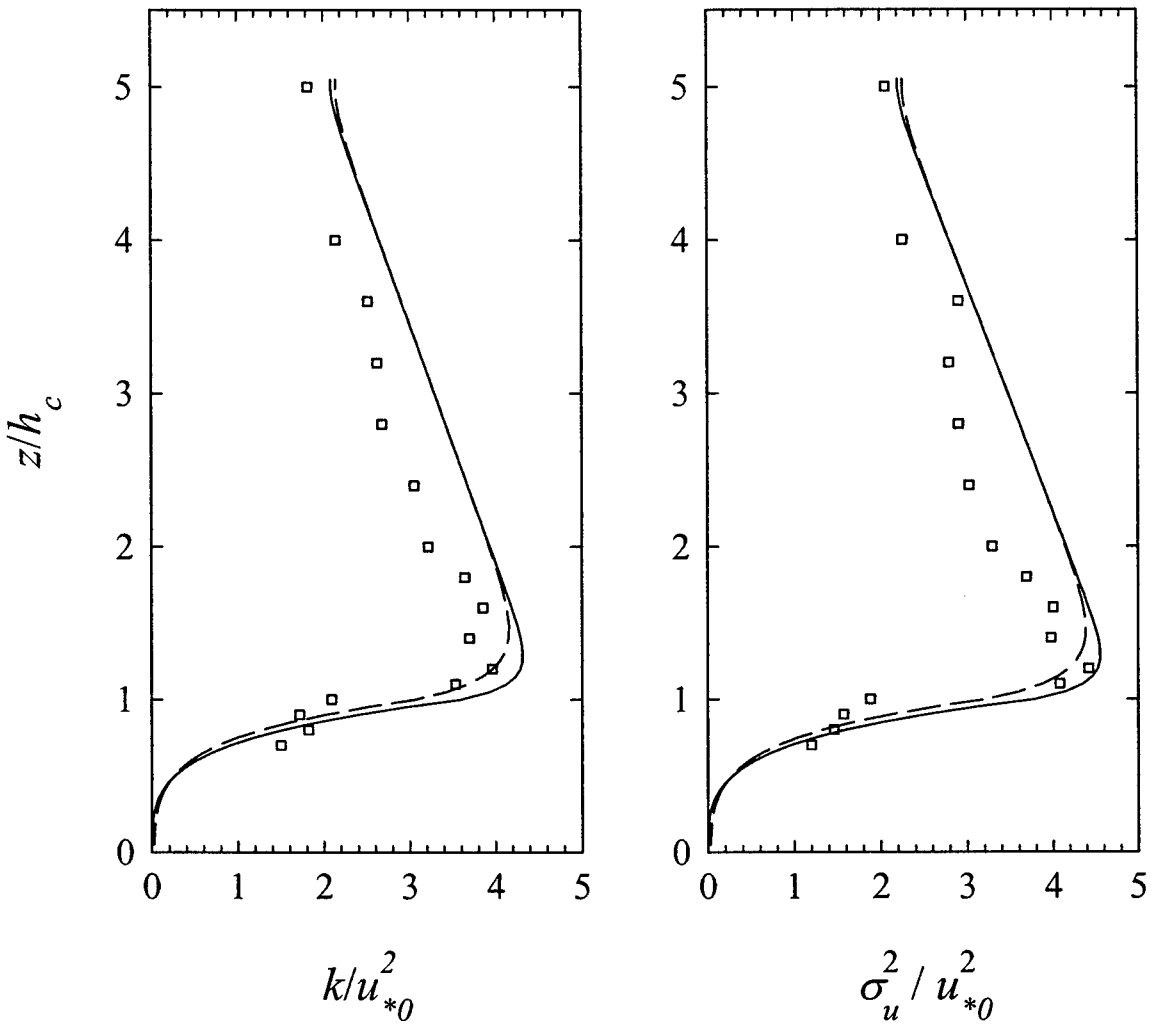

Figure 21. *Turbulence kinetic energy (left panel) and streamwise velocity variance (right panel) observed in and above a staggered array of cubical obstacles with a frontal area index of 0.44 compared with the outcome of model simulations using the basic (solid curve) and alternative (long dashed curve) canopy windflow models.*

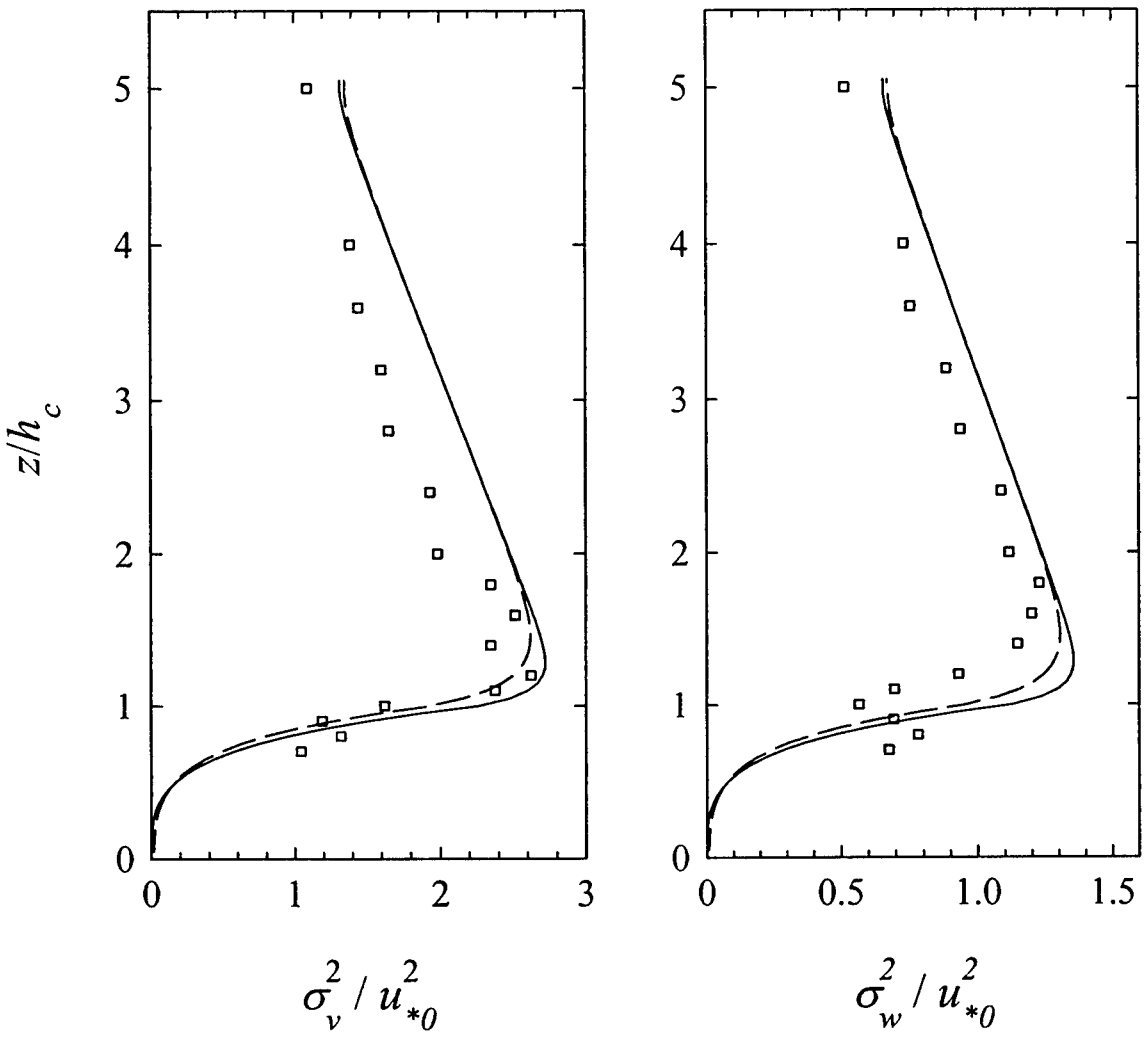

Figure 22. *Cross-stream velocity variance (left panel) and vertical velocity variance (right panel) observed in and above a staggered array of cubical obstacles with a frontal area index of 0.44 compared with the outcome of model simulations using the basic (solid curve) and alternative (long dashed curve) canopy windflow models.*

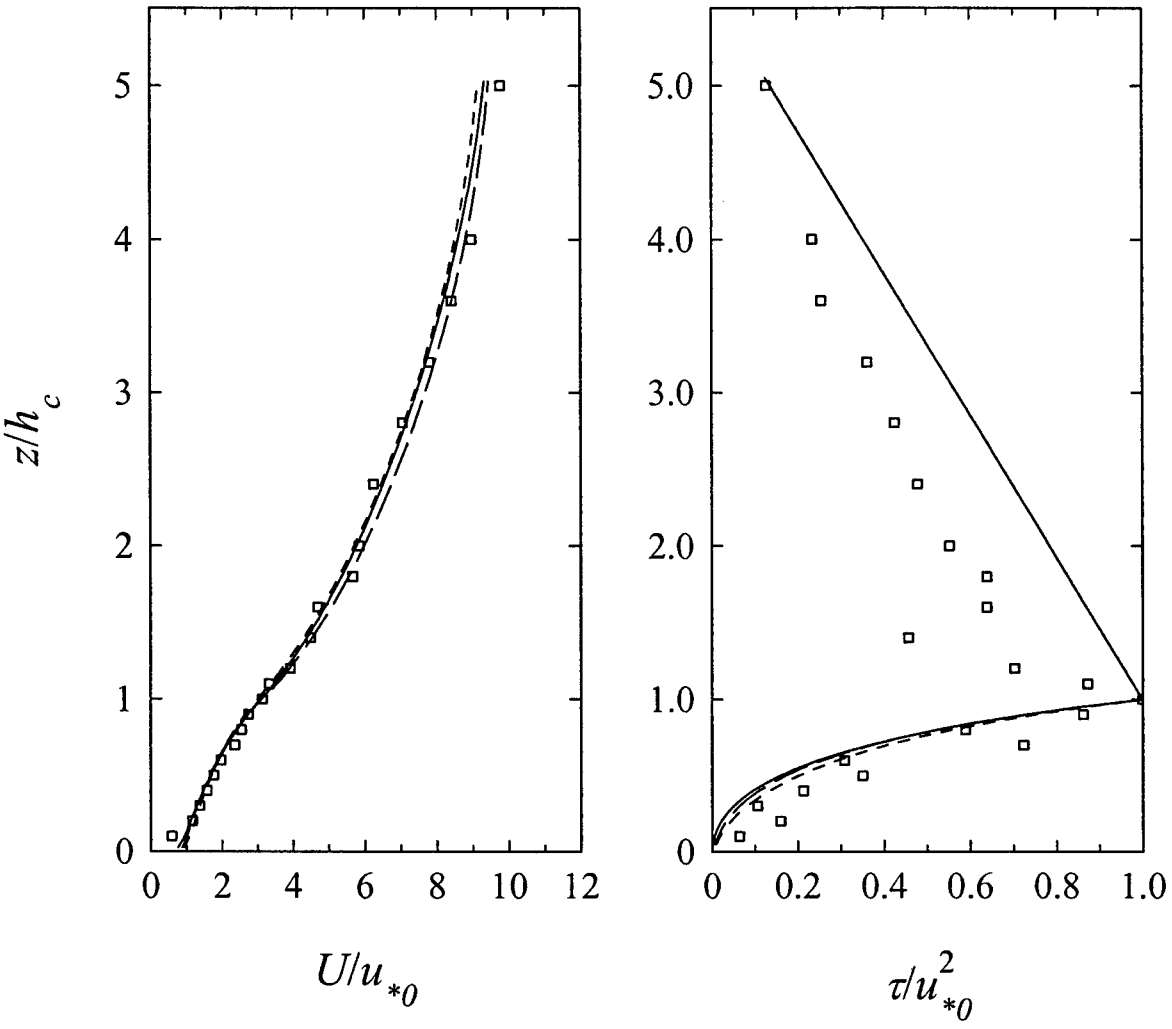

Figure 23. *Mean wind speed (left panel) and shear stress (right panel) observed in and above a square array of billboard-shaped obstacles with a frontal area index of 0.16 compared with the outcome of model simulations using the basic (solid curve) and alternative (long dashed curve) canopy windflow models. The short dashed curve corresponds to a model simulation using the alternative windflow model with the form drag sink for TKE eliminated.*

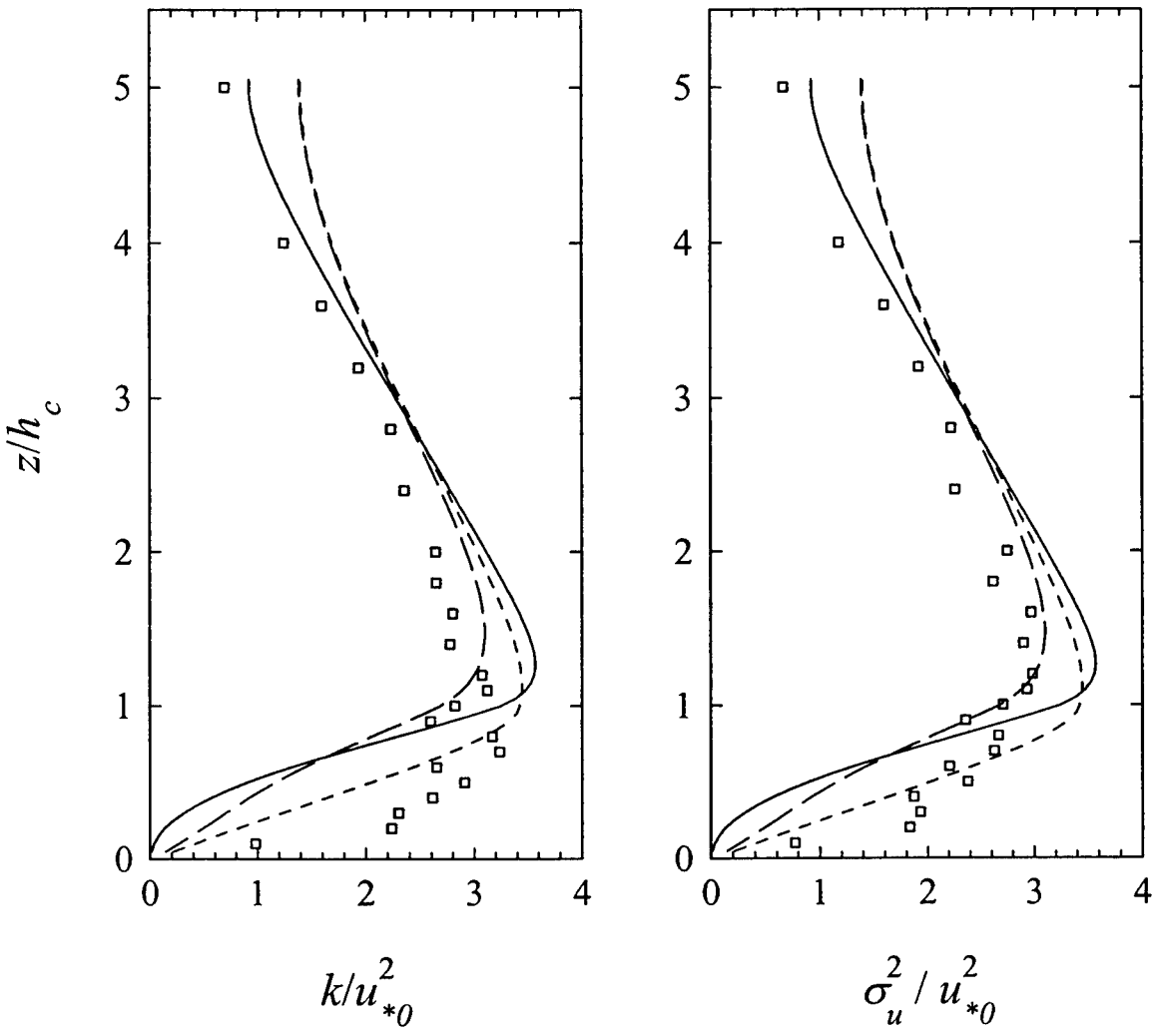

Figure 24. *Turbulence kinetic energy (left panel) and streamwise velocity variance (right panel) observed in and above a square array of billboard-shaped obstacles with a frontal area index of 0.16 compared with the outcome of model simulations using the basic (solid curve) and alternative (long dashed curve) canopy windflow models. The short dashed curve corresponds to a model simulation using the alternative windflow model with the form drag sink for TKE eliminated.*

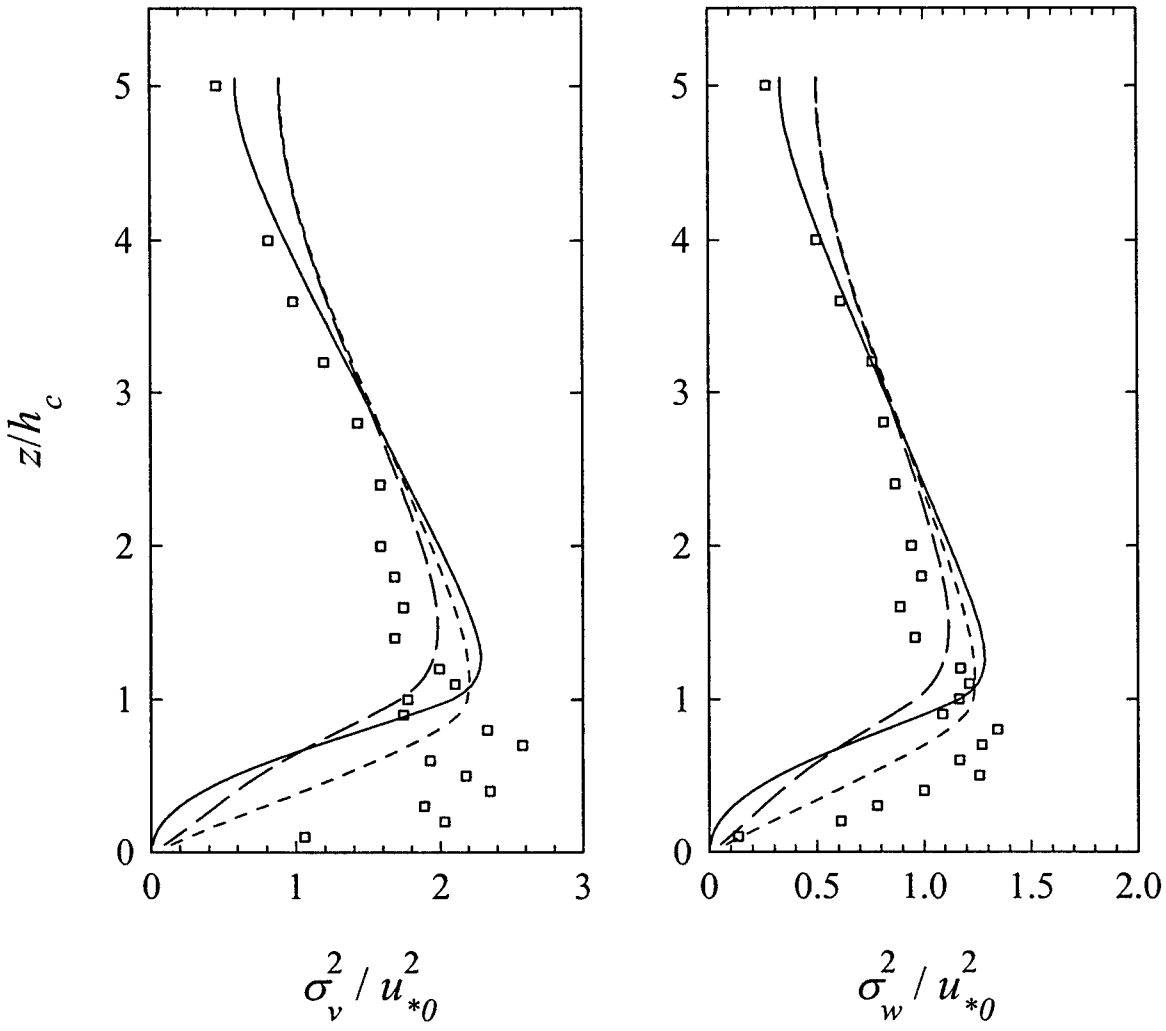

Figure 25. *Cross-stream velocity variance (left panel) and vertical velocity variance (right panel) observed in and above a square array of billboard-shaped obstacles with a frontal area index of 0.16 compared with the outcome of model simulations using the basic (solid curve) and alternative (long dashed curve) canopy windflow models. The short dashed curve corresponds to a model simulation using the alternative windflow model with the form drag sink for TKE eliminated.*

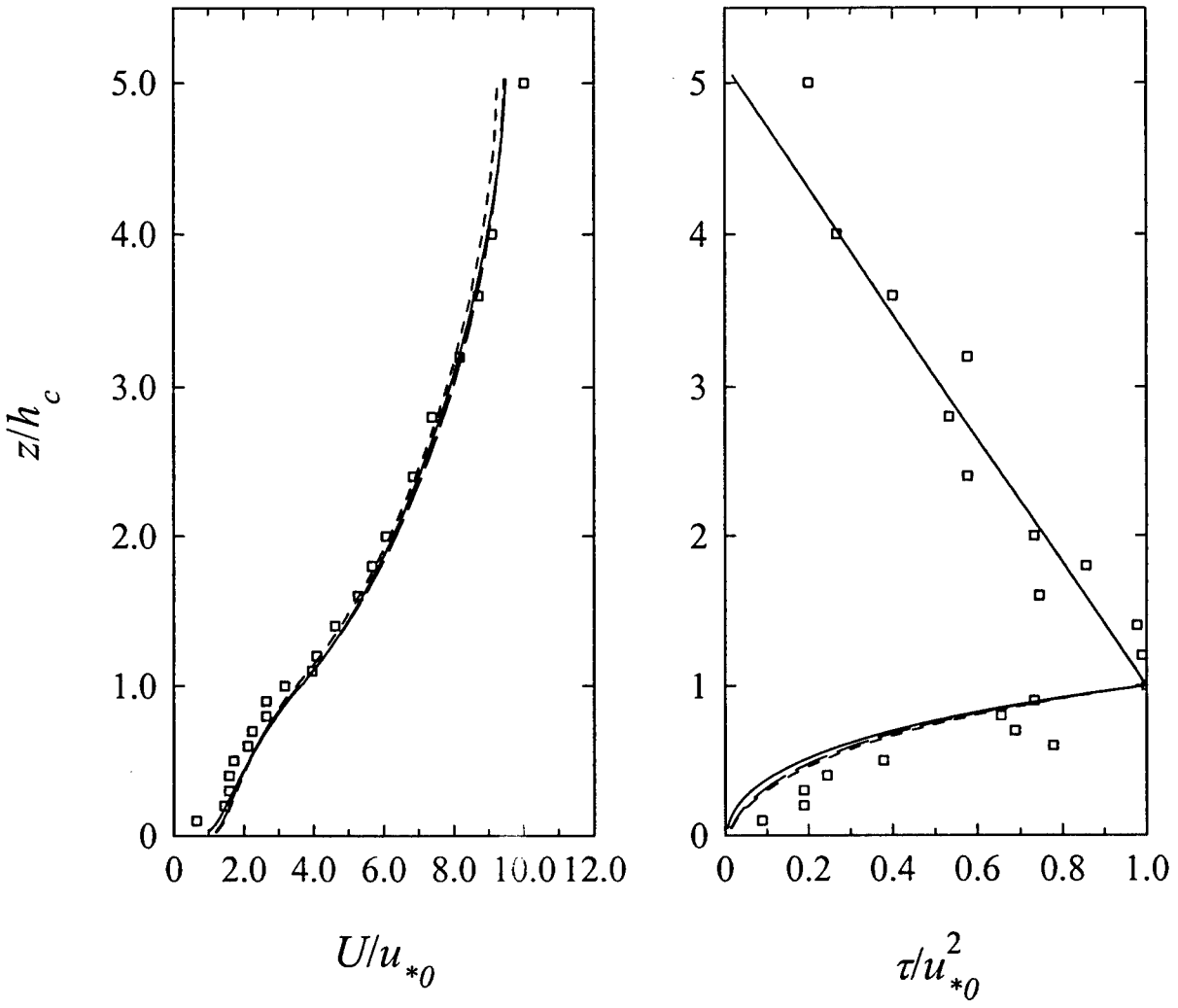

Figure 26. *Mean wind speed (left panel) and shear stress (right panel) observed in and above a staggered array of billboard-shaped obstacles with a frontal area index of 0.16 compared with the outcome of model simulations using the basic (solid curve) and alternative (long dashed curve) canopy windflow models. The short dashed curve corresponds to a model simulation using the alternative windflow model with the form drag sink for TKE eliminated.*

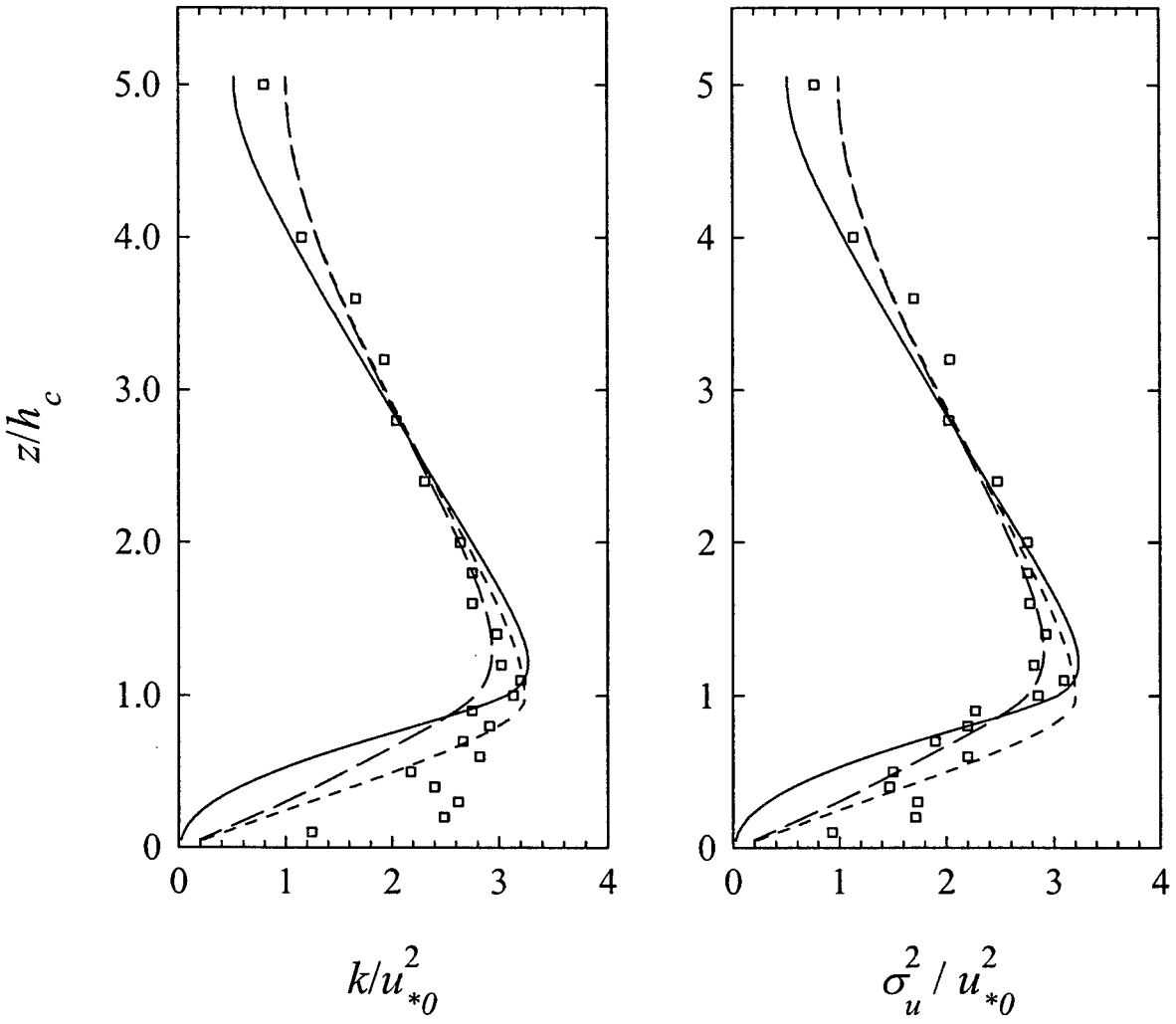

Figure 27. *Turbulence kinetic energy (left panel) and streamwise velocity variance (right panel) observed in and above a staggered array of billboard-shaped obstacles with a frontal area index of 0.16 compared with the outcome of model simulations using the basic (solid curve) and alternative (long dashed curve) canopy windflow models. The short dashed curve corresponds to a model simulation using the alternative windflow model with the form drag sink for TKE eliminated.*

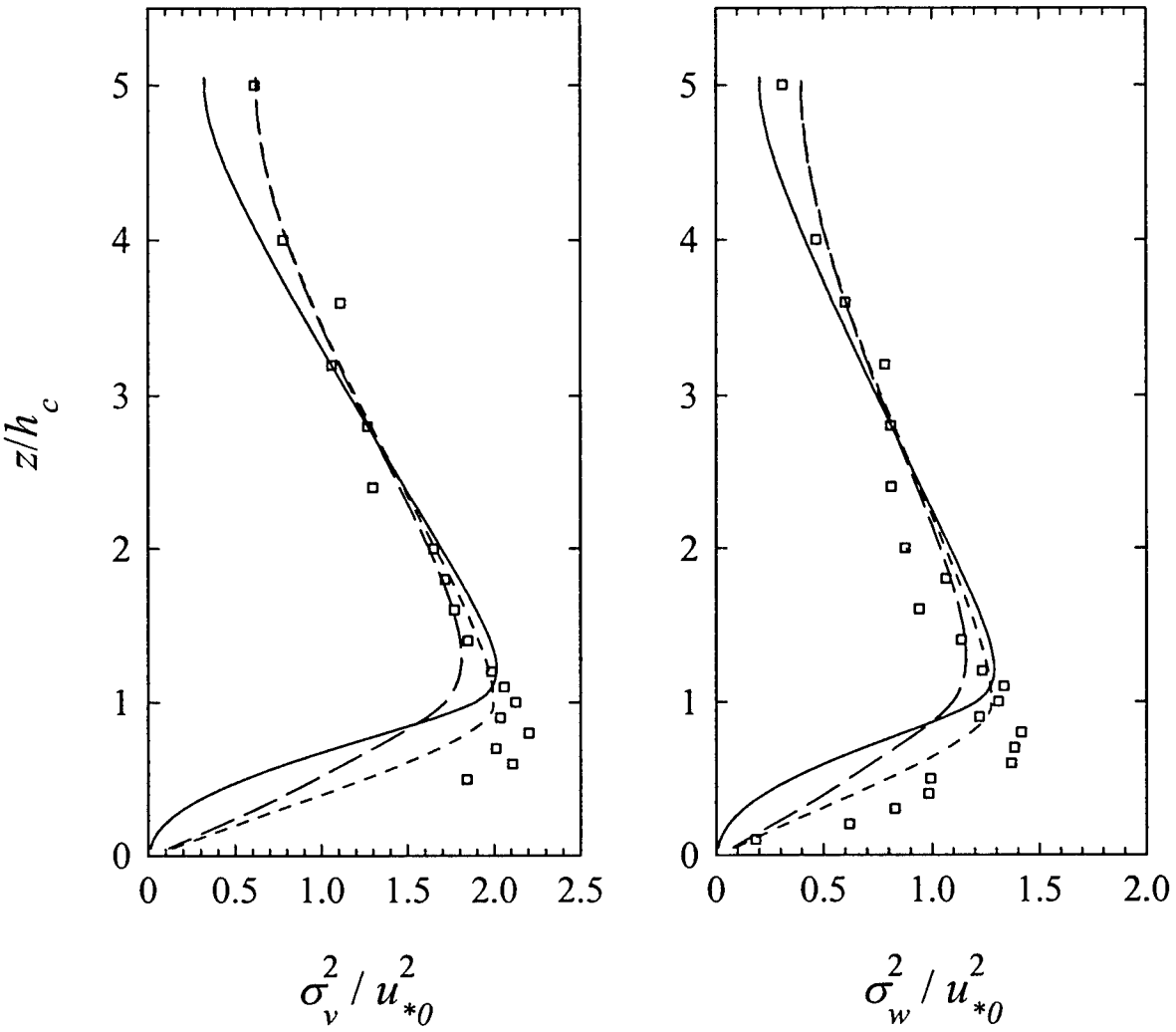

Figure 28. *Cross-stream velocity variance (left panel) and vertical velocity variance (right panel) observed in and above a staggered array of billboard-shaped obstacles with a frontal area index of 0.16 compared with the outcome of model simulations using the basic (solid curve) and alternative (long dashed curve) canopy windflow models. The short dashed curve corresponds to a model simulation using the alternative windflow model with the form drag sink for TKE eliminated.*

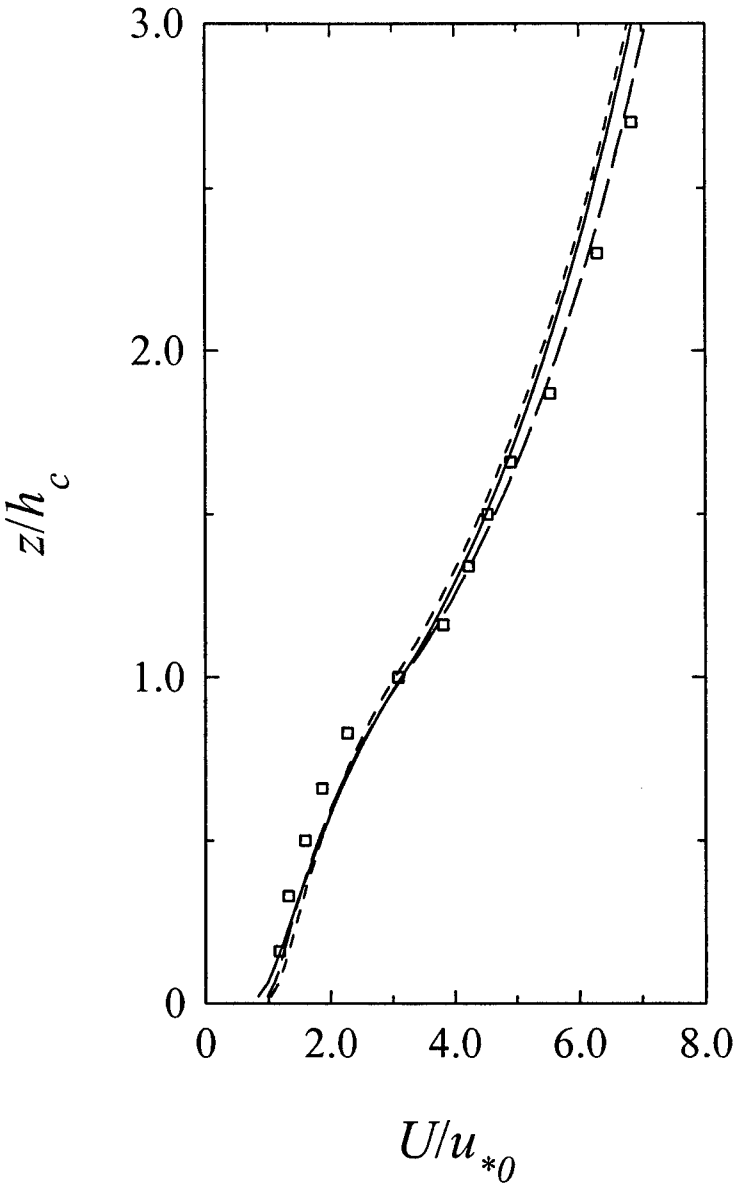

Figure 29. *Mean wind speed observed in and above a model canopy of staggered flat plates with frontal area index of 0.23 (Tombstone canopy) compared with the outcome of model simulations using the basic (solid curve) and alternative (long dashed curve) canopy windflow models. The short dashed curve corresponds to a model simulation with the alternative windflow model with the form drag sink for TKE eliminated.*

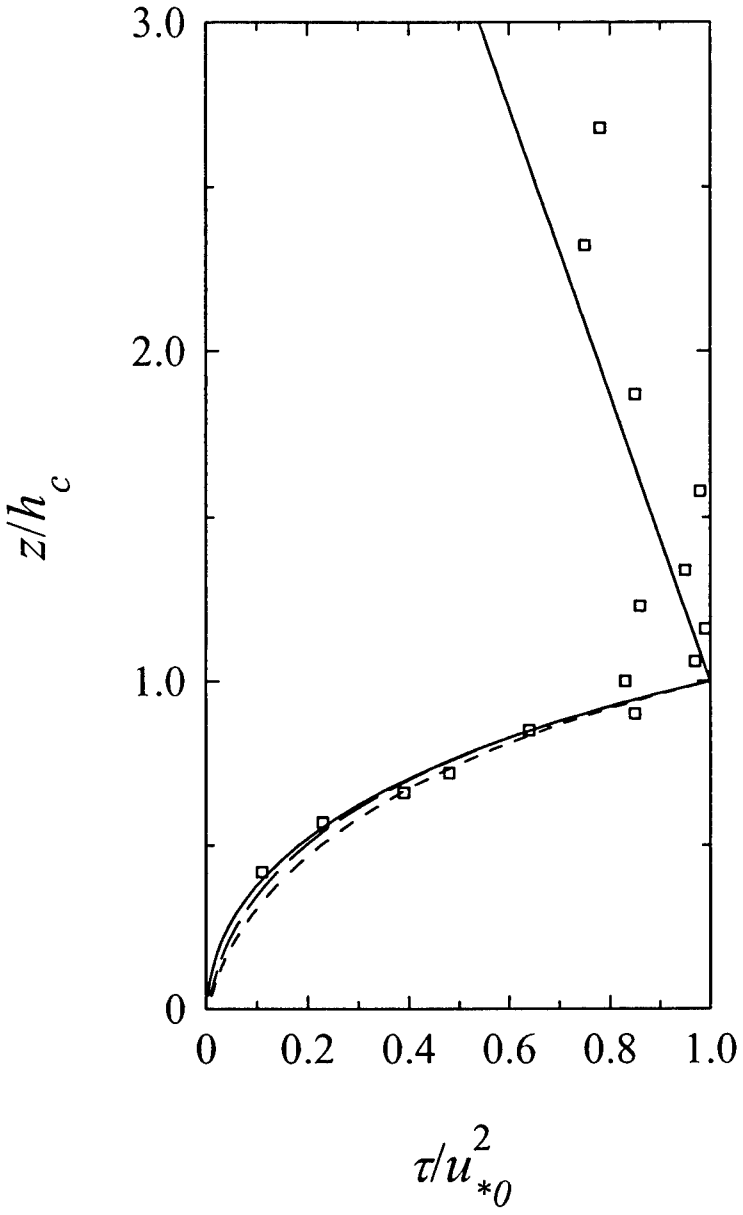

Figure 30. *Shear stress observed in and above a model canopy of staggered flat plates with frontal area index of 0.23 (Tombstone canopy) compared with the outcome of model simulations using the basic (solid curve) and alternative (long dashed curve) canopy windflow models. The short dashed curve corresponds to a model simulation with the alternative windflow model with the form drag sink for TKE eliminated.*

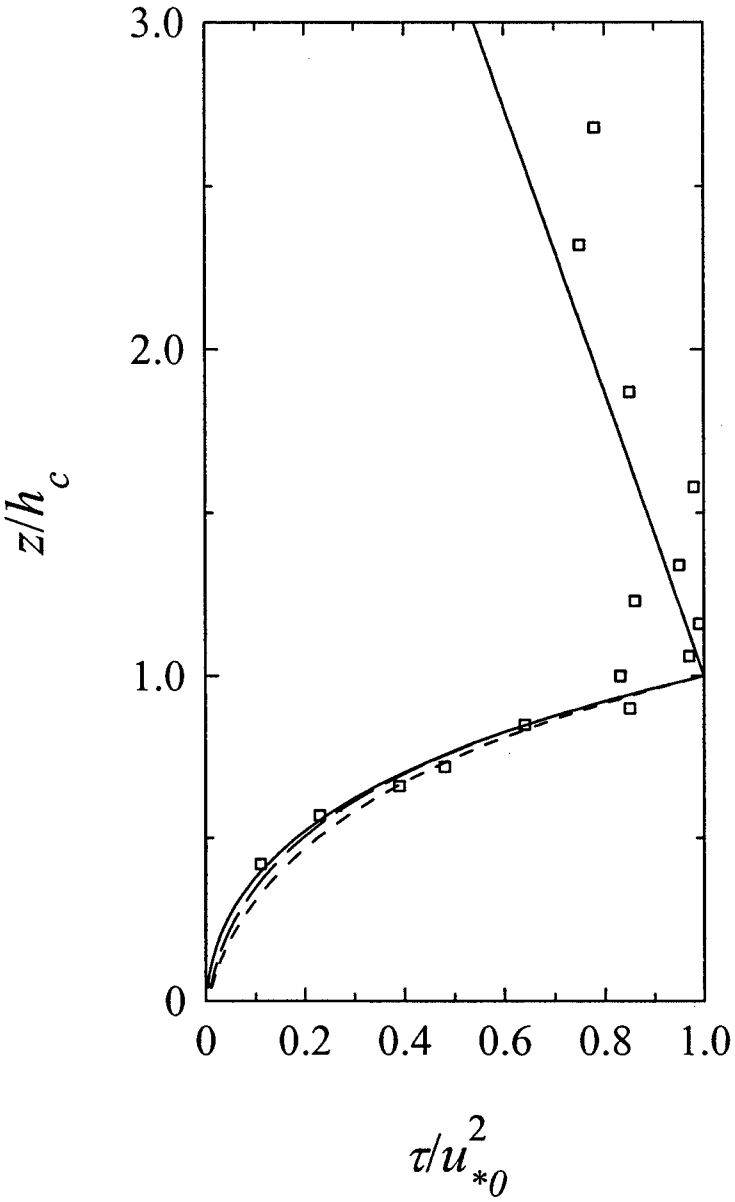

Figure 31. *Turbulence kinetic energy observed in and above a model canopy of staggered flat plates with frontal area index of 0.23 (Tombstone canopy) compared with the outcome of model simulations using the basic (solid curve) and alternative (long dashed curve) canopy windflow models. The short dashed curve corresponds to a model simulation with the alternative windflow model with the form drag sink for TKE eliminated.*

DOCUMENT CONTROL DATA

(Security classification of title, body of abstract and indexing annotation must be entered when the overall document is classified)

1. ORIGINATOR (the name and address of the organization preparing the document. Organizations for whom the document was prepared, e.g. Establishment sponsoring a contractor's report, or tasking agency, are entered in section 8.)

Defence Research Establishment Suffield
P.O. Box 4000
Medicine Hat, Alberta T1A 8K6

2. SECURITY CLASSIFICATION (overall security classification of the document. including special warning terms if applicable)

UNCLASSIFIED

3. TITLE (the complete document title as indicated on the title page. Its classification should be indicated by the appropriate abbreviation (S,C,R or U) in parentheses after the title.)

A Comparison Between a First-Order Model for Disturbed Urban Canopy Flows with Observations for Mean Wind and Turbulence (U)

4. AUTHORS (Last name, first name, middle initial. If military, show rank, e.g. Doe, Maj. John E.)

Yee, Eugene and Wilson, J.D.

5. DATE OF PUBLICATION (month and year of publication of document)	6a. NO. OF PAGES (total containing information. Include Annexes, Appendices, etc.)	6b. NO. OF REFS (total cited in document)
December 2001	77	27

6. DESCRIPTIVE NOTES (the category of the document, e.g. technical report, technical note or memorandum. If appropriate, enter the type of report, e.g. interim, progress, summary, annual or final. Give the inclusive dates when a specific reporting period is covered.)

Technical Report (Final) [1 January, 2001 to 1 May, 2001]

8. SPONSORING ACTIVITY (the name of the department project office or laboratory sponsoring the research and development. Include the address.)

Defence Research Establishment Suffield
P.O. Box 4000
Medicine Hat, Alberta T1A 8K6

9a. PROJECT OR GRANT NO. (if appropriate, the applicable research and development project or grant number under which the document was written. Please specify whether project or grant)	9b. CONTRACT NO. (if appropriate, the applicable number under which the document was written)
PCN No. 6QD11	

10a. ORIGINATOR'S DOCUMENT NUMBER (the official document number by which the document is identified by the originating activity. This number must be unique to this document.)	10b. OTHER DOCUMENT NOS. (Any other numbers which may be assigned this document either by the originator or by the sponsor)
DRES TR 2001-058	

11. DOCUMENT AVAILABILITY (any limitations on further dissemination of the document, other than those imposed by security classification)

(X) Unlimited distribution
( ) Distribution limited to defence departments and defence contractors; further distribution only as approved
( ) Distribution limited to defence departments and Canadian defence contractors; further distribution only as approved
( ) Distribution limited to government departments and agencies; further distribution only as approved
( ) Distribution limited to defence departments; further distribution only as approved
( ) Other (please specify):

12. DOCUMENT ANNOUNCEMENT (any limitation to the bibliographic announcement of this document. This will normally correspond to the Document Availabilty (11). However, where further distribution (beyond the audience specified in 11) is possible, a wider announcement audience may be selected.)

No

13. ABSTRACT (a brief and factual summary of the document. It may also appear elsewhere in the body of the document itself. It is highly desirable that the abstract of classified documents be unclassified. Each paragraph of the abstract shall begin with an indication of the security classification of the information in the paragraph (unless the document itself is unclassified) represented as (S), (C), (R), or (U). It is not necessary to include here abstracts in both offical languages unless the text is bilingual).

Two canopy windflow models (basic model and alternative model) are described and assessed against measurements of mean wind and turbulence in a wide range of canopies (both vegetative and urban). The windflow models are based on a first-order turbulence closure for the description of both the mean wind (U) and kinetic energy of turbulence (k), viz. Reynolds' equations are closed using eddy-viscosity $K \sim \lambda k^{1/2}$, where λ is an algebraically specified turbulence length scale. The windflow models are compared with eleven different canopy flows (aeroelastic plant canopy; corn canopy; square and staggered arrays of cubical obstacles at three different frontal area densities [0.0625, 0.16, and 0.44]; square and staggered arrays of billboard-shaped obstacles at a frontal area density of 0.16; and, the Tombstone canopy). Comparisons of model predictions with these different canopies show that the alternative windflow model gives the best overall conformance with respect to both mean flow and turbulence profiles. The basic windflow model was found to underpredict the turbulence kinetic energy within the canopy, although this underprediction does not appear to affect its reasonably good predictions of the mean wind speed and the shear stress. However, both the basic and alternative windflow models underpredict severely the magnitude of the mean wind shear at the canopy top for for ``urban" canopies at the highest frontal area density [0.44] investigated. It is suggested that the alternative windflow model can be used probably unmodified (viz., without resorting to tuning of any model constants) for the simulation of a wide range of canopy flows provided the frontal area densities of the ``urban" canopies are not so large as to provoke skimming flow.

14. KEYWORDS, DESCRIPTORS or IDENTIFIERS (technically meaningful terms or short phrases that characterize a document and could be helpful in cataloguing the document. They should be selected so that no security classification is required. Identifiers, such as equipment model designation, trade name, military project code name, geographic location may also be included. If possible keywords should be selected from a published thesaurus. e.g. Thesaurus of Engineering and Scientific Terms (TEST) and that thesaurus-identified. If it is not possible to select indexing terms which are Unclassified, the classification of each should be indicated as with the title.)

Canopy Windflow Modeling
Vegetative and Urban Canopies
Computational Fluid Dynamics
Model Validation

Defence R&D Canada
is the national authority for providing
Science and Technology (S&T) leadership
in the advancement and maintenance
of Canada's defence capabilities.

R et D pour la défense Canada
est responsable, au niveau national, pour
les sciences et la technologie (S et T)
au service de l'avancement et du maintien des
capacités de défense du Canada.

www.drdc-rddc.dnd.ca

Executive summary

Introduction: It is anticipated that Canadian Forces (CF) in the foreseeable future will have to fight in or protect urban areas, whether in battle, peace-making, peace-keeping, or counter-terrorist operations. The increased awareness and importance accorded by the public worldwide and their governments to maintain appropriate defences against chemical and biological (CB) agents in an urban (built-up) environment, the prediction of casualties and human performance degradation resulting from such releases, and the development of operational procedures and regulations to control, mitigate, and monitor the fate of CB agents in urban areas with high population densities, will require mathematical modeling of urban wind flows and dispersion. In this regard, it should be noted that the prediction of urban canopy flow is in principle pre-requisite to or co-requisite with the prediction of the simpler (but itself complex) problem of scalar (e.g., CB agent) dispersion within a canopy.

Results: Two canopy windflow models (basic model and alternative model) are described and assessed against measurements of mean wind and turbulence in a wide range of canopies (both vegetative and urban). The windflow models are based on a first-order turbulence closure for the description of both the mean wind (U) and kinetic energy of turbulence (k), viz. Reynolds' equations are closed using eddy-viscosity $K \sim \lambda k^{1/2}$, where λ is an algebraically specified turbulence length scale. The windflow models are compared with eleven different canopy flows (aeroelastic plant canopy; corn canopy; square and staggered arrays of cubical obstacles at three different frontal area densities [0.0625, 0.16, and 0.44]; square and staggered arrays of billboard-shaped obstacles at a frontal area density of 0.16; and, the Tombstone canopy). Comparisons of model predictions with these different canopies show that the alternative windflow model gives the best overall conformance with respect to both mean flow and turbulence profiles. The basic windflow model was found to underpredict the turbulence kinetic energy within the canopy, although this underprediction does not appear to affect its reasonably good predictions of the mean wind speed and the shear stress. However, both the basic and alternative windflow models underpredict severely the magnitude of the mean wind shear at the canopy top for for "urban" canopies at the highest frontal area density [0.44] investigated. It is suggested that the alternative windflow model can be used probably unmodified (viz., without resorting to tuning of any model constants) for the simulation of a wide range of canopy flows provided the frontal area densities of the "urban" canopies are not so large as to provoke skimming flow.

Significance and Future Plans: The canopy windflow models considered in this report provide all the statistics of the wind field (i.e., spatial variation of the mean wind velocity, Reynolds stresses, and viscous dissipation rate over the urban landscape) required as the

input to drive a physically-based model for the prediction of urban dispersion. An example of such a physically-based model is the Lagrangian Stochastic (LS) model. This model requires that the turbulent velocity field, viz. mean velocity, velocity variances, shear stresses, and the Lagrangian time scale (or, equivalently, the viscous dissipation rate), be supplied as the external inputs. The implication of the differences between various windflow models for mean velocity, velocity variances, and viscous dissipation rate should be tested in a Lagrangian dispersion model to determine the sensitivity of predicted tracer concentrations to the windflow model predictions of mean flow and turbulence.

Yee, E. and Wilson, J. D., 2001. A Comparison Between a First-Order Closure Model for Disturbed Urban Canopy Flows with Observations for Mean Wind and Turbulence. DRES TR 2001–058, Defence Research Establishment Suffield.